Sex differences in NK cells mediated by the X-linked epigenetic regulator UTX

Mandy I. Cheng[1,2,], Luke Riggan[1,2,], Joey H. Li[1,2], Rana Yakhshi Tafti[1,2], Scott Chin[1], Feiyang Ma[3,4], Matteo Pellegrini[3,4], Haley Hrncir[6], Arthur P. Arnold[6], Timothy E. O'Sullivan[1,2,*] and Maureen A. Su[1,2,5,*]

[1]Department of Microbiology, Immunology, and Molecular Genetics, David Geffen School of Medicine at UCLA, Los Angeles, CA 90095
[2]Molecular Biology Institute, University of California, Los Angeles, Los Angeles, CA 90095, USA
[3]Department of Molecular, Cell, and Developmental Biology, University of California, Los Angeles, California, USA.
[4]Institute for Genomics and Proteomics, University of California, Los Angeles, California, USA.
[5]Department of Pediatrics, David Geffen School of Medicine at UCLA, Los Angeles, CA 90095
[6]Department of Physiological Science, Laboratory of Neuroendocrinology of the Brain Research Institute, University of California, Los Angeles, CA 90095-1606, USA.
[*]Corresponding Authors

Correspondence:

Timothy E. O'Sullivan, PhD
David Geffen School of Medicine at UCLA
615 Charles E. Young Drive South, BSRB 245F
Los Angeles, CA 90095
Phone: 310-825-4454
Email: tosullivan@mednet.ucla.edu

Maureen A. Su, MD
David Geffen School of Medicine at UCLA
615 Charles E. Young Drive South, BSRB 290C
Los Angeles, CA 90095
Phone: 310-825-2130
Email: masu@mednet.ucla.edu

Abstract

Viral infection outcomes are sex-biased, with males generally more susceptible than females. Paradoxically, the numbers of anti-viral natural killer (NK) cells are increased in males compared to females. Using samples from mice and humans, we demonstrate that while numbers of male NK cells are increased compared to females, they display impaired production of the anti-viral cytokine IFN-γ. These sex differences were not due solely to divergent levels of gonadal hormones, since these differences persisted in gonadectomized mice. Instead, these differences can be attributed to lower male expression of X-linked *Kdm6a* (UTX), an epigenetic regulator which escapes X inactivation in female NK cells. NK cell-specific UTX deletion in females phenocopied multiple features of male NK cells, which include increased numbers and reduced IFN-γ production. Integrative ATAC-seq and RNA-seq analysis revealed a critical role for UTX in the regulation of chromatin accessibility and gene expression at loci important in NK cell homeostasis and effector function. Consequently, NK cell-intrinsic UTX levels are critical for optimal anti-viral immunity, since mice with NK cell-intrinsic UTX deficiency show increased lethality to mouse cytomegalovirus (MCMV) challenge. Taken together, these data implicate UTX as a critical molecular determinant of NK cell sex differences and suggest enhancing UTX function as a new strategy to boost endogenous NK cell anti-viral responses.

60 **Introduction**

61 Evolutionarily conserved sex differences exist in both innate and adaptive immune responses[1,2].
62 While males are less susceptible to autoimmunity, they also mount a limited anti-viral immune
63 response compared to females[3]. For instance, males have a higher human cytomegalovirus
64 (HCMV) burden after infection, suggesting increased susceptibility to viral threats[4]. This has
65 also been recently illustrated with the COVID-19 pandemic, in which the strong male bias for
66 severe disease has been postulated to reflect sex differences in immune responses[5]. Multiple
67 studies in humans and mice have recently reported differences in immune cell distribution
68 and/or function in males vs. females[6-10]. However, the molecular basis for these differences, and
69 the mechanisms by which these differences influence disease outcomes, remain incompletely
70 understood.

71 Sex differences in mammals are defined not only by divergent gonadal hormones, but
72 also by sex chromosome dosage[1]. Expression of a subset of X-linked genes, for example, is
73 higher in females (XX) than males (XY). While females undergo random X chromosome
74 inactivation (XCI) to maintain similar levels of X-linked protein expression between sexes, XCI
75 is incomplete, with 3-7% of X chromosome genes escaping inactivation in mice and 20-30%
76 escaping inactivation in humans[11]. As such, differential levels of X-linked gene expression in
77 females vs. males have been linked to sex differences in a wide range of conditions including
78 neural tube defects[12] and autoimmune disease[13].

79 As circulating type 1 innate lymphocytes, NK cells serve as an early line of defense
80 against herpesvirus family members[14]. The importance of NK cells in anti-viral immunity is
81 illustrated in patients with defective NK cell numbers or functionality, who are highly susceptible
82 to infection by herpesviruses, such as HCMV and Epstein-Barr virus (EBV)[15,16]. Similarly, NK
83 cells are required for the control of mouse cytomegalovirus (MCMV) and other viral infections[17-
84 19], as mice with either genetic deficiency in NK cell function or loss of NK cell numbers have a

85 significant increase in viral titers and mortality following MCMV infection[20-25]. Thus, NK cells are
86 critical in anti-viral immunity across species.

87 Given this role for NK cells, it was therefore unexpected that NK cells are increased in
88 virus-susceptible males[6-10]. Beyond NK cell numbers, other previously unappreciated sexually
89 dimorphic NK cell feature(s) may instead account for sex differences with viral infections. Here,
90 we show that NK cells in males are simultaneously expanded in number and deficient in effector
91 function across mice and humans. These sex differences in NK cell composition and function
92 are not completely due to hormonal differences, since these differences persisted in
93 gonadectomized mice. Through expression screening, we identified the epigenetic regulator
94 UTX (encoded by gene *Kdm6a*) as an XCI escapee that is expressed at significantly lower
95 levels in male NK cells across mice and humans. Conditional ablation of UTX in female mouse
96 NK cells, which mimics lower UTX expression in male NK cells, recapitulated NK cell
97 phenotypes associated with male sex, such as increased NK cell numbers and lower production
98 of IFN-γ. Furthermore, parallel Assay for transposase-accessible chromatin using sequencing
99 (ATAC-seq) and bulk RNA sequencing (RNA-seq) of WT and UTX^{NKD} NK cells revealed a
100 critical role for UTX in regulating chromatin accessibility and transcription of gene clusters
101 involved in NK cell fitness (*Bcl2*) and effector response (*Ifng and Csf2).* Notably, UTX^{NKD} mice
102 had increased mortality in response to MCMV infection, suggesting a critical role for UTX in the
103 production of optimal anti-viral effector responses. Ultimately, our findings demonstrate that
104 divergent UTX levels underlie sex differences in NK cell homeostasis and effector function.
105 Enhancing UTX function may therefore represent a novel strategy for optimizing NK cell-
106 mediated anti-viral immunity.
107
108
109
110

111 **Results**

112 **NK cells display sexually dimorphic phenotypes independent of gonadal sex hormones.**

113 Due to the critical role of NK cells in anti-viral immunity and increased male susceptibility to
114 cytomegalovirus (CMV) and other herpesvirus family infections[4], it was surprising that multiple
115 studies have reported that human males display increased NK cell numbers[6-10]. A recent
116 investigation examining spleens of C57BL/6 mice also reported increased numbers of NK cells
117 in males vs. females[26]. Consistent with this, our data show that splenic NK cells are increased in
118 frequency **(Fig. 1a,b)** and absolute numbers **(Fig. 1c)** in male C57BL/6 mice compared to
119 females. These findings suggest that other sexually dimorphic features beyond NK cell numbers
120 may account for increased male susceptibility to viral infections. In response to viral infection,
121 NK cells are critical for early production of proinflammatory cytokines, particularly IFN-γ[27]. To
122 test if sex differences exist in NK cell-intrinsic function, we compared effector cytokine
123 production in NK cells from female vs. male mice *ex vivo*. Stimulation with IL-12 and IL-18,
124 cytokines known to induce robust IFN-γ production by NK cells[28], resulted in lower IFN-γ
125 production by male NK cells **(Fig. 1d-f)**. Similarly, stimulation of activated human NK cells
126 ($TCR\beta^-$ $CD3^-$ $CD56^+$) isolated from peripheral blood mononuclear cells (PBMCs) with IL-12 and
127 K562 leukemia cells resulted in lower %IFN-γ^+ **(Fig. 1g)** and IFN-γ MFI **(Fig. 1h)** in male
128 compared to female NK cells**.** Thus, while NK cell numbers are increased, male NK cell effector
129 function is consistently reduced in both mice and humans.

130 Female or male sex is based on a composite of gonadal hormones (e.g., estrogens or
131 androgens) and sex chromosomes (e.g., 46XX or 46XY)[1]. Previous studies demonstrated direct
132 effects of gonadal hormones in regulation of IFN-γ production by NK cells[29], but it remains
133 possible that NK cell sex differences can also be attributed to sex chromosome complement. To
134 test this possibility, we gonadectomized mice to abolish the effect of sex hormones.
135 Gonadectomy failed to eliminate sex differences in NK cell frequency **(Fig. 1i),** absolute
136 numbers **(Fig. 1j)** and IFN-γ protein production in response to cytokine stimulation **(Fig. 1k)**,

137 indicating that gonadal hormones are not solely responsible for sex differences in NK cells.
138 Thus, we hypothesized that chromosomal complement, in particular X chromosome dosage,
139 may also play an important role.
140
141 **X-linked UTX escapes X-inactivation and has higher expression in female NK cells.**
142 While 46XX females undergo X chromosome inactivation (XCI) to control dosages of X-linked
143 genes, a subset of genes escapes XCI (termed XCI escapees), often resulting in higher
144 expression in females compared to males. Thus, XCI escapees are prime candidates for
145 mediating phenotypic sex differences in NK cells. Five genes (*XIST*, *DDX3X, KDM6A, EIF2S3,*
146 *KDM5C*) have previously been identified as XCI escapees in both humans and mice[30]. *XIST*
147 was excluded from further analysis because it is not expressed in male cells due to its known
148 role in X chromosome inactivation in female cells[1]. All 4 remaining genes were significantly
149 downregulated in male vs. female NK cells, from humans **(Fig. 2a)** and mice **(Fig. 2b).** The
150 greatest differential expression in both human and mouse NK cells was seen with *Kdm6a* (also
151 known as UTX*)* **(Fig. 2a,b**). Male NK cells also expressed lower UTX protein levels compared to
152 female NK cells in mice **(Fig. 2c,d)**. These data indicate that expression levels of *Kdm6a* (UTX)
153 is sex-biased in NK cells.
154 In NK cells derived from gonadectomized mice, differences persisted in *Kdm6a*
155 transcript levels **(Fig. 2e)** and UTX protein levels **(Fig. 2f).** Additionally, using the four core
156 genotype (FCG) mouse model, which uncouples sex chromosome complement (XX or XY) and
157 gonadal sex organ (ovaries or testes)[31], *Kdm6a* transcript levels were also lower in mice with
158 one X chromosome (XY) independent of gonadal composition **(Extended Data Fig. 2a)**.
159 Together these findings suggest that increased UTX expression in female mice is not due to
160 hormonal effects and instead point to a primary role for X chromosome dosage.
161
162

163 **UTX deletion recapitulates male NK cell phenotypes of frequency and IFN-γ production.**
164 To determine if UTX mediates sex differences in NK cells, we generated mice with a conditional
165 deletion of UTX in NK cells (*Kdm6a*$^{fl/fl}$ x *Ncr1*$^{Cre+}$, referred to as UTX^{NKD} hereafter) with WT
166 (*Kdm6a*$^{fl/fl}$ x *Ncr1*$^{Cre-}$) littermates used as controls. To control for gonadal hormone and sex
167 chromosome effects, comparisons were made only in female mice (female WT vs. female
168 UTX^{NKD} littermates). We confirmed decreased UTX protein expression in NK cells from UTX^{NKD}
169 mice using flow cytometry **(Extended Data Fig. 2b,c).** Similar to male mice, female UTX^{NKD}
170 mice displayed increased splenic NK cell frequency **(Fig. 3a,b)** and absolute numbers **(Fig. 3c)**
171 in the spleen, blood, lungs, liver and bone marrow, demonstrating that this increase was not
172 tissue specific. Furthermore, IFN-γ protein production in response to IL-12 and IL-18 stimulation
173 was decreased in NK cells from UTX^{NKD} vs. WT mice **(Fig. 3d-f)**. These results implicate UTX in
174 limiting NK cell numbers and promoting IFN-γ production, suggesting divergent UTX levels may
175 play a causal role in NK cell sex differences.

176

177 **Global changes in NK cell chromatin accessibility and transcription mediated by UTX**

178 Recent studies have identified NK cell regulatory circuitry (regulomes) that prime innate
179 lymphoid cells for swift effector responses even prior to NK cell activation[32,33]. As an epigenetic
180 modifier, UTX can alter transcription by organizing chromatin at regulatory elements of target
181 gene loci[34]. To investigate the UTX-mediated modifications on chromatin accessibility and gene
182 expression in NK cells, we performed Assay for Transposase-Accessible Chromatin using
183 sequencing (ATAC-seq) in tandem with bulk RNA sequencing (RNA-seq) on sort-purified WT
184 (CD45.1^{+}) and UTX^{NKD} (CD45.2^{+}) NK cells from WT:UTX^{NKD} mixed bone marrow chimeras
185 (mBMCs) **(Fig. 4a)**. Using mBMCs allowed for an internally controlled experiment to minimize
186 environmental confounding factors. Principle Component Analysis (PCA) of both ATAC-seq and
187 RNA-seq data revealed that samples clustered together by genotype **(Fig. 4b)**, indicating that

188 loss of UTX results in profound changes in both the chromatin landscape and transcriptome of
189 NK cells. ATAC-seq revealed 3569 peaks decreased and 2113 peaks increased in accessibility
190 in UTX^{NKD} compared to WT NK cells (Log_2 Fold Change > ±0.5, adjusted p-value < 0.05, FDR <
191 0.05) **(Supplementary Table 1)**. Moreover, RNA-seq identified 577 decreased and 377
192 increased genes in UTX^{NKD} vs. WT (Log_2 Fold Change > ± 0.5, adjusted p-value < 0.05, FDR <
193 0.05) **(Supplementary Table 2)**. Thus, these data suggest UTX plays an active role in
194 controlling the NK regulome at baseline.

195 Integrative analysis of ATAC-seq and RNA-seq identified 400 genes that are both
196 differentially accessible and expressed with a significant positive correlation (Spearman
197 correlation: $R = 0.62$, $p < 2.2x10^{-16}$) between the mean log_2 fold change of ATAC-seq peaks and
198 log_2 fold change of RNA-seq expression **(Extended Data Fig. 3a)**. Fuzzy c-means clustering[35]
199 of both the ATAC-seq and RNA-seq datasets identified six major clusters which were
200 significantly decreased (Clusters 1, 2, 3, and 6) or increased (Clusters 4 and 5) in accessibility
201 (**Fig. 4c)** and expression **(Fig. 4d)** in UTX^{NKD} NK cells. For functional enrichment analysis,
202 g:Profiler[36] was used to analyze clusters of differentially expressed genes identified by RNA-seq
203 **(Fig. 4e)**. Major pathways such as immune system process, cytokine production, IFN-γ
204 production, lymphocyte activation, and immune effector process were associated with
205 decreased expression in UTX^{NKD} (Clusters 1, 2, 3, and 6) **(Fig. 4e)**. At the same time, pathways
206 such as developmental process, biosynthetic process, and metabolic process were significantly
207 associated with increased expression in UTX^{NKD} (Clusters 4 and 5) **(Fig. 4e)**. Collectively, these
208 findings implicate UTX in the coordinate regulation of genes associated with NK cell
209 homeostasis and effector function.

210 Furthermore, UTX is known to interact with transcription factors (TFs) to coordinate
211 target gene transcription[34]. To identify putative UTX TF partners, we performed HOMER
212 (Hypergeometric Optimization of Motif Enrichment)[37] TF motif analysis on each cluster of

213 significant differentially accessible peaks **(Fig. 4f)**. TFs associated with modulating effector
214 function during viral infection such as Runt (Runx1 and Runx2)[38] and T-box (Eomes, T-bet, Tbr1
215 and Tbx6)[39] family TFs were more significant and had a higher percentage of target motifs
216 associated with clusters displaying decreased accessibility in UTX^{NKD} (Clusters 1, 2, 3, and 6)
217 **(Fig. 4f)**. Conversely, TFs associated with proliferation, differentiation, and metabolism in the
218 zinc finger family TFs (KLF1, KLF5, KLF6, KLF14, Sp2 and Sp5)[40] were more significantly
219 associated with clusters displaying increased accessibility (Clusters 4 and 5) **(Fig. 4f)**. These
220 data suggest that UTX poises the chromatin accessibility of several genes at steady state
221 known to influence NK cell fitness and effector responses, while also controlling genome-wide
222 accessibility of transcription factor binding sites implicated in these processes.

223

224 **UTX coordinately regulates chromatin accessibility and expression of apoptosis pathway**
225 **genes.**

226 The observed expansion of NK cell numbers in UTX^{NKD} mice **(Fig. 3a-c)** could either be due to
227 higher NK cell proliferation or increased resistance to apoptosis. However, UTX^{NKD} NK cells
228 paradoxically displayed a lower proportion of cells expressing the cell division marker Ki67
229 **(Extended Data Fig. 4a).** UTX^{NKD} NK cells also showed less CFSE dilution in response to IL-15,
230 a cytokine known to induce NK cell proliferation **(Extended Data Fig. 4b,c)**. Thus, these results
231 suggest that higher NK cell numbers observed in UTX^{NKD} mice were not due to increased
232 proliferation. In contrast, increased survival is likely the cause of expanded NK cell numbers in
233 UTX^{NKD} mice.

234 Among the differentially accessible and expressed genes in NK cells lacking UTX were
235 those important in controlling apoptosis. An anti-apoptotic gene, *Bcl2,* showed increased
236 accessibility and expression in UTX^{NKD} vs. WT NK cells (**Fig.5a, Extended Data Fig. 3b**).
237 Previous studies in mice have demonstrated that Bcl-2 can inhibit the pro-apoptotic function of

238 Bim to promote NK cell survival[41], thus, we interrogated the expression of these proteins in
239 UTX^{NKD} NK cells. While naïve UTX^{NKD} NK cells showed increased intracellular protein
240 expression of Bcl-2 compared to WT NK cells **(Fig. 5b,d),** UTX-deficient NK cells also displayed
241 a modest increase in intracellular Bim levels **(Fig. 5c,e)**. Importantly, the Bcl-2:Bim ratio was
242 significantly higher in UTX^{NKD} NK cells **(Fig. 5f)**, suggesting UTX-deficiency likely results in a
243 higher proportion of pro-survival proteins present in NK cells. Notably, male NK cells also
244 displayed a significant increase in Bcl-2:Bim ratio, which may underlie the expanded NK cell
245 numbers observed in male mice **(Fig. 5g)**. These results implicate UTX in regulation of NK cell
246 fitness to restrict numbers at homeostasis.

247

248 **UTX is critical for NK cell IFN-γ production and effector function.**

249 Since NK cells are early responders to MCMV, rapid effector molecule production is critical for
250 NK cell mediated anti-viral control. ATAC-seq and RNA-seq of NK cells from WT:UTX^{NKD}
251 mBMCs identified various chromatin accessibility and transcript changes at steady state **(Fig.**
252 **4b,c)**. Specifically, genes involved in the NK effector response (*Ifng* and *Csf2)*[27,42] showed
253 decreased accessibility and expression in UTX^{NKD} compared to WT NK cells **(Fig. 6a, Extended**
254 **data fig. 3b-d)**. Moreover, qRT-PCR verified decreases in *Ifng* transcript levels in UTX^{NKD} vs.
255 WT NK cells at rest **(Fig. 6b).** Similarly, male NK cells, which express lower levels of UTX
256 **(Fig.2c,d),** also had a similar decrease in *Ifng* transcript levels at rest **(Fig. 6c)**. Thus, through
257 shaping of the chromatin landscape, UTX controls levels of effector gene transcripts available
258 prior to immune challenge.

259 To determine whether UTX deficiency also led to decreased chromatin accessibility and
260 transcription of effector genes in NK cells during infection, we performed ATAC-seq on NK cells
261 isolated from MCMV-infected WT:UTX^{NKD} mBMCs on D1.5 post-infection (PI). Similar to naïve
262 UTX-deficient NK cells, D1.5 PI UTX^{NKD} NK cells also showed decreased chromatin accessibility

263 at the *Ifng* and *Csf2* loci **(Fig. 6d,e, Extended Data Fig. 3e,f)**. qRT-PCR confirmed decreased
264 *Ifng* and *Csf2* transcripts in NK cells from UTX^{NKD} mice at D1.5 PI **(Fig. 6f)**. Similarly, UTX^{NKD}
265 NK cells showed decreased IFN-γ protein expression in UTX^{NKD} NK cells on D1.5 PI indicating
266 that UTX expression in NK cells is required for optimal IFN-γ production following viral infection
267 **(Fig. 6g,h)**. To confirm whether dosage of UTX expression in mature NK cells associates with
268 NK cell production of IFN-γ during viral infection, we generated transgenic mice to achieve
269 tamoxifen-inducible UTX deletion (*Rosa26*$^{ERT2CRE/+}$ x *Kdm6a*$^{fl/fl}$: $iUTX^{-/-}$). Tamoxifen
270 administration in WT:$iUTX^{-/-}$ mBMCs resulted in differential degrees of UTX protein loss, and
271 displayed a positive correlation between intracellular UTX levels and IFN-γ production on D1.5
272 PI **(Extended Data Fig. 5).** Since IFN-γ production by NK cells is critical for protection against
273 MCMV[27], we challenged WT and UTX^{NKD} mice with a sublethal dose of MCMV and monitored
274 survival. While WT mice controlled MCMV infection (n = 8/8 survived), UTX^{NKD} mice rapidly
275 succumbed to infection (n = 3/8 survived) **(Fig. 6i)**. These results demonstrate a requirement for
276 NK cell-intrinsic UTX in the control of effector molecule production and protection against
277 MCMV infection.
278
279
280
281
282
283
284
285

286 **Discussion**

287 Sex is a critical biological variable in determining outcomes to viral infections[3]. This was recently
288 illustrated with COVID-19, in which male sex was identified as a major risk factor for severe
289 disease[5]. Moreover, recent studies have linked NK cell dysfunction within severe COVID-19
290 disease[43]. Given the importance of NK cells in anti-viral immunity, understanding the root
291 causes of sex differences in NK cell biology will have far-reaching implications in optimizing anti-
292 viral immunity. In this study, we demonstrated that lower expression of UTX in XX UTX^{NKD} NK
293 cells mimics levels in XY NK cells, which may contribute to increased NK cell numbers and
294 decreased IFN-γ production in males **(Extended Data Fig. 6a)**. UTX is expressed at lower
295 levels in male NK cells across mice and human and this observation is independent of gonadal
296 hormones in mice. NK cell UTX is required for controlling NK cell fitness, modulating
297 accessibility of transcription factor binding motifs, increasing chromatin accessibility at effector
298 gene loci, and poising NK cells for rapid response to virus infection **(Extended Data Fig. 6b)**.
299 Together, these findings support a model in which divergent UTX expression contributes to sex
300 differences in NK cell numbers and effector function.

301 Our findings indicate that UTX restricts NK cell numbers at steady state, since NK cells
302 are increased at baseline in UTX^{NKD} mice. This is in contrast to UTX deficiency in other immune
303 cell types, which have been reported to result in moderate ($CD8^+$ and $CD4^+$ T cells) or severe
304 (iNKT) decreases in peripheral cell numbers[44-46]. Interestingly, T cell-specific UTX-deficiency is
305 associated with $CD8^+$ T cell accumulation during viral infection. Thus, it is possible that UTX-
306 mediated gene programs that inhibit $CD8^+$ T cell numbers during inflammation are shared by NK
307 cells at rest[46]. Indeed, increased Bcl-2 levels were observed in both UTX-deficient NK cells and
308 UTX-deficient $CD8^+$ T cells, suggesting that UTX down-regulates this anti-apoptotic factor in
309 both innate and adaptive cytotoxic lymphocytes.

310 NK cell-mediated effector functions during viral infection include cytokine production
311 (IFN-γ) and cytotoxic molecule expression[47]. Our results from simultaneous ATAC-seq and

312 RNA-seq suggest that UTX poises the chromatin landscape of NK cells at rest to quickly
313 respond to viral challenge by increasing accessibility and transcription of effector loci such as
314 *Ifng* and *Csf2* prior to viral infection[27,42]. Decreased IFN-γ protein levels were seen at D1.5 post
315 MCMV-infection in UTX-deficient NK cells, suggesting decreased effector functionality during
316 inflammation. These results support a previous study that suggests the existence of an NK cell
317 regulome[27,42], in which NK cell chromatin accessibility is actively maintained at steady-state and
318 demonstrates a critical role for UTX in its maintenance before and during inflammation.

319 As a histone demethylase, UTX has intrinsic catalytic ability to demethylate H3K27me3
320 (a repressive histone mark) to poise chromatin for active gene expression[48]. In addition to its
321 catalytic activity, UTX functions in multiprotein complexes with other epigenetic regulators (e.g.
322 SWI/SNF, MLL4/5 and p300) to mediate chromatin remodeling in a demethylase-independent
323 manner[48,49]. In $CD8^+$ T cells, UTX binds to enhancer and TSS of effector genes to promote
324 effector gene programs in a demethylase-independent manner[46]. In contrast, demethylase
325 activity in iNKT cells is required for the development and function and H3K27 methylation
326 correlated with gene programs important for $CD4^+$ T follicular helper cell development[44,50]. Thus,
327 the molecular mechanisms by which UTX functions appears to be immune cell specific. A
328 previous study treated human NK cells with a small molecule inhibitor of H3K27me3
329 demethylases (GSK-J4) and found reduced cytokine expression (IFN-γ, TNF-α, GM-CSF, and
330 IL-10) in response to *in vitro* stimulation[51]. However, GSK-J4 is not a specific tool for studying
331 UTX-mediated mechanisms because it also inhibits Jmjd3, another H3K27me3 demethylase as
332 well as having non-specific effects on other histone demethylases[52]. Thus, further studies using
333 more precise genetic modification strategies are needed to understand the mechanisms by
334 which UTX functions in NK cells.

335 UTX has been reported to interact with lineage specific TFs in T cells to target particular
336 effector loci[34]. Our studies using HOMER motif analysis revealed potential interactions between

337 UTX and TFs associated with modulating NK cell effector function during viral infection (Runx1,
338 Runx2, Eomes, T-bet, Tbr1, and Tbx6). Moreover, these analyses also point to UTX interactions
339 with TFs associated with NK cell proliferation, differentiation, and metabolism (KLF1, KLF5,
340 KLF6, KLF14, Sp2 and Sp5). In line with a physiologic role for TFs in UTX-mediated control of
341 chromatin accessibility, TF binding motifs were strongly enriched in ATAC-seq gene clusters.
342 Further studies will be needed to experimentally verify these interactions in mouse and human
343 NK cells.

344 NK cells are critical for control of HCMV infection in humans because NK cell-deficient
345 individuals develop disseminated herpesvirus infections[16,53]. Sex differences in immune
346 response to multiple viruses have been reported, including immune responses to HCMV[53]. Our
347 data support a model in which sex differences in anti-viral immunity can partially be explained
348 by differences in UTX expression in NK cells, given the increased susceptibility of UTX^{NKD} mice
349 to MCMV challenge. UTX deficiency has also been associated with Kabuki Syndrome and
350 Turner Syndrome[44,54], two human conditions associated with immune dysregulation and
351 increased infections. Our findings suggest the possibility that UTX deficiency in human NK cells
352 may contribute to decreased viral immunosurveillance observed in these patients, although
353 future work will be needed to support this hypothesis.

354 Weighing factors that define patient subsets with different immune responses will allow
355 us to move past a “one-size-fits-all” therapeutic approach to a precision medicine paradigm.
356 Understanding sex differences in NK cell function and their molecular underpinnings is an
357 important step toward incorporating sex as a biological factor in treatment decisions. In males
358 with severe viral illness, for instance, enhancing NK cell UTX activity may provide therapeutic
359 benefit. We expect that these insights will be important not only in the setting of viral infections,
360 but also in other infections and cancer, where NK cells also play an important role. These

361 findings may also have important implications for adoptive cellular therapies, in which NK cells
362 are the subject of intense interest[55,56].
363
364 **Acknowledgements**
365 We thank members of the O'Sullivan and Su labs for helpful discussion. We thank the UCLA
366 Technology Center for Genomics and Bioinformatics for RNA sequencing library preparation
367 and the Cedars Sinai Applied Genomics, Computation, and Translational Core Facility for ATAC
368 sequencing library preparation. T.E.O. is supported by the NIH (AI145997) and UC CRCC
369 (CRN-20-637105). M.A.S. is supported by the NIH (NS107851, AI143894, DK119445)
370 Department of Defense (USAMRAA PR200530), and National Organization of Rare Diseases.
371 M.I.C. is supported by Ruth L. Kirschstein National Research Service Awards (GM007185 and
372 AI007323), and Whitcome Fellowship from the Molecular Biology Institute at UCLA. L.R. is
373 supported by the Warsaw fellowship from the MIMG department at UCLA. J.H.L. is supported
374 by the NIH NIAMS (T32AR071307). A.P.A. is supported by NIH HD100298.
375
376 **Author Contributions**
377 M.I.C., L.R., J.H.L., R.Y.T., H.H., A.P.A., T.E.O. and M.A.S. designed the study; M.I.C., J.H.L.,
378 R.Y.T., L.R., and S.C. performed the experiments; M.I.C., R.T.Y., F.M., and M.P. performed
379 bioinformatics analysis; M.A.S, M.I.C. and T.E.O. wrote the manuscript.
380
381 **Competing Interests Statement**
382 T.E.O. is a scientific advisor for Xyphos Inc., a company that has financial interest in human NK
383 cell-based therapeutics.

Figure 1

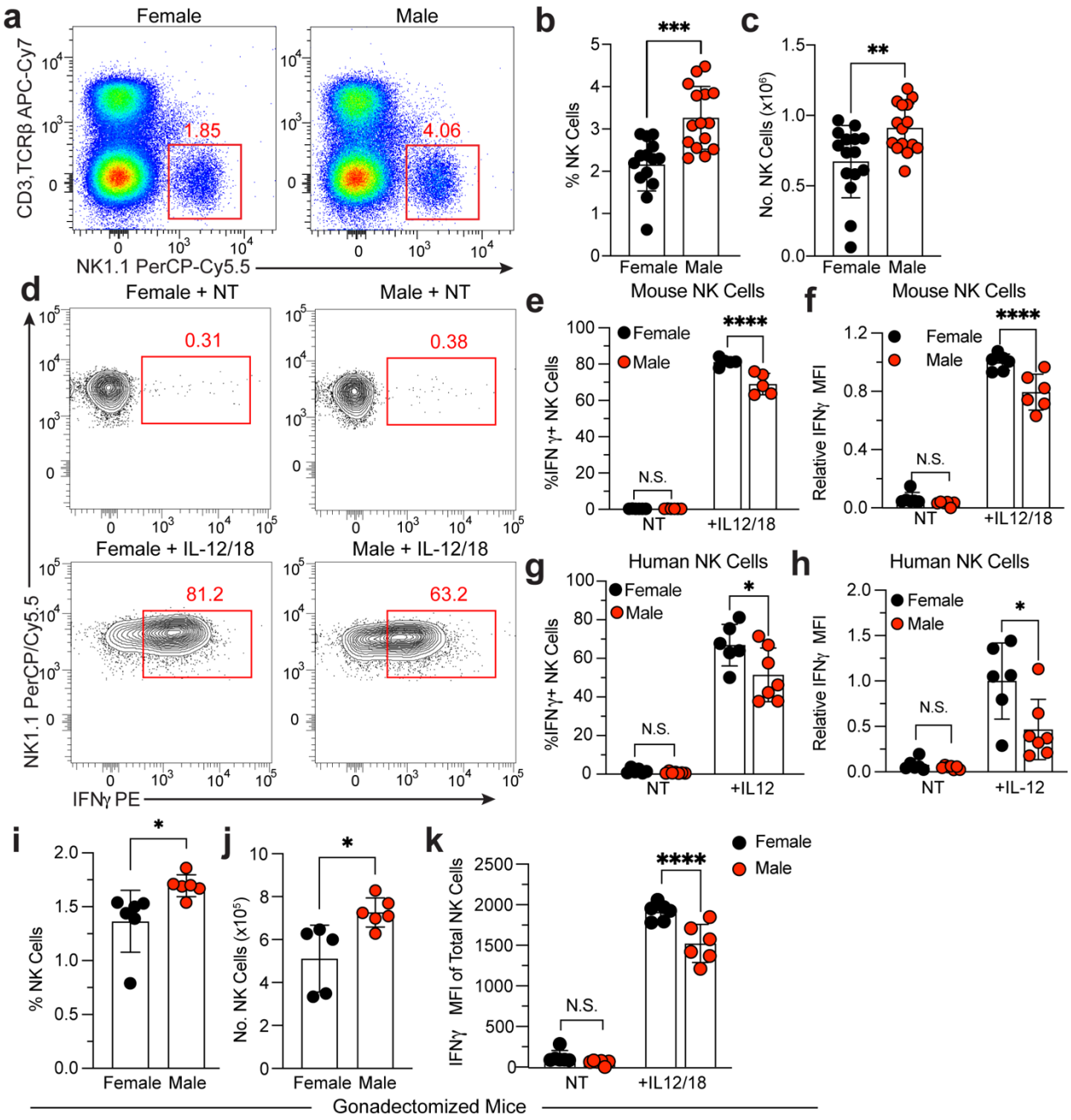

Figure 1: Sex differences in IFN-γ production and NK cell numbers in mouse and human NK cells are independent of gonadal hormones. a) Representative dot plots, **b)** percentage, and **c)** absolute numbers of splenic NK cells ($CD3^-$ $TCR\beta^-$ $NK1.1^+$) in female and male C57BL/6 mice (n = 15 per group). **d)** Representative contour plots, and bar graphs depicting **e)** percentages IFN-γ^+ and **f)** relative IFN-γ mean fluorescence intensity (MFI) of total NK cells with

390 no treatment (NT) or in response to IL-12 (20 ng/ml) and IL-18 (10 ng/ml) stimulation of splenic
391 NK cells from female vs. male mice for 5 hours *ex vivo* (n = 5 per group, data representative of
392 2 independent experiments, normalized to female IL-12/18 treatment). **(g-h)** Human NK cells
393 isolated from peripheral blood of female (n = 6) and male (n = 7) donors were cultured and
394 stimulated with 10 ng/ml of IL-12 for 16 hours in the presence of K562 cells. **g)** Percentage of
395 IFN-γ^+ NK cells, and **h)** relative MFI of IFN-γ in TCRβ^-CD3$^-$CD56$^+$ female and male human NK
396 cells (normalized to female IL-12 treatment). **i)** Frequency and **j)** absolute numbers of splenic
397 NK cells identified in gonadectomized mice (n = 6 per group). **k)** IFN-γ MFI of total splenic NK
398 cells isolated gonadectomized female and male mice stimulated with IL-12 (20 ng/ml) and IL-18
399 (10 ng/ml) for 5 hours *ex vivo* (n = 6 per group). Samples were compared using two-tailed
400 Student's t test and data points are presented as individual mice with the mean ± SEM (N.S.,
401 Not Significant; *, $p < 0.05$; **, $p < 0.01$; ***, $p<0.001$; ****, $p<0.0001$).
402
403

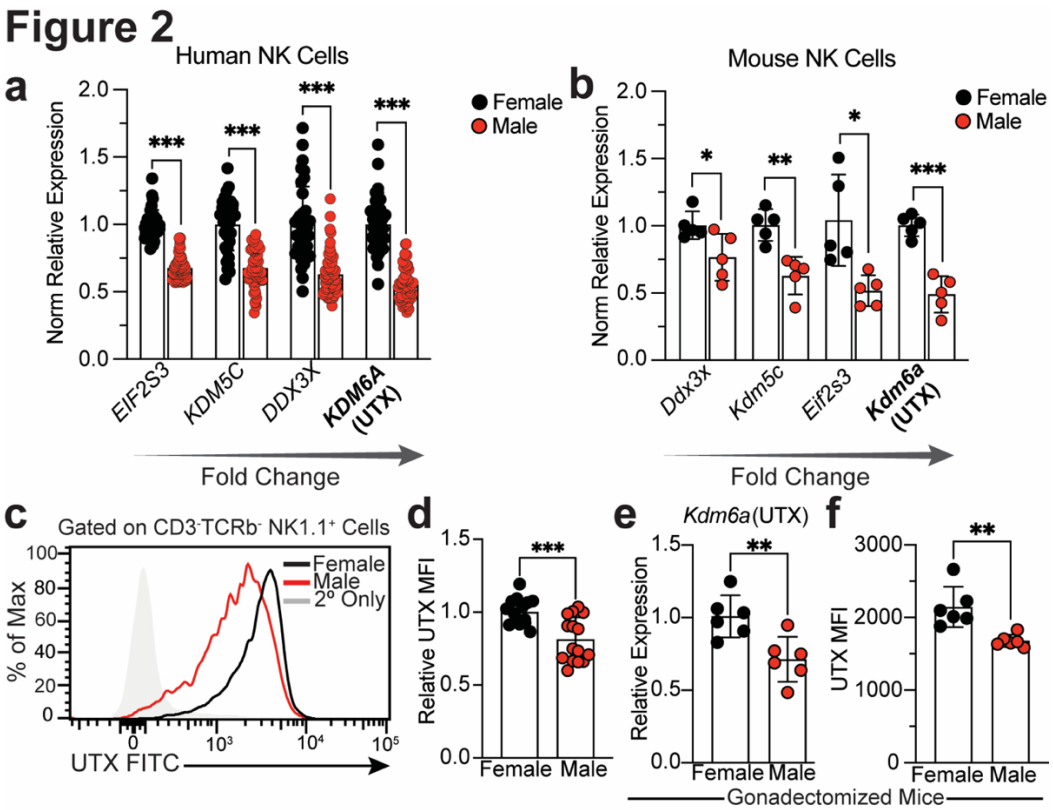

Figure 2: X-linked UTX displays sexually dimorphic gene expression independent of sex hormones. a) Relative expression of X-chromosome inactivation escapee genes using DICE database which performed RNA-seq on sorted NK cells from human females (n = 36) vs. males (n = 54) normalized to female. **b)** Relative expression of X chromosome inactivation escapee genes by RT-qPCR in NK cells from female vs. male mice (C57BL/6; 8 week old, n = 5 per group). Genes are ordered by increasing fold change. **c)** Representative histogram and **b)** relative MFI of UTX protein expression in splenic NK cells from naïve female vs. male mice by flow cytometry (C57BL/6; 8 week old). **e)** Relative expression of *Kdm6a* (UTX) by RT-qPCR of isolated splenic NK cells normalized to female and **f)** UTX MFI of NK cells by flow cytometry from spleens of gonadectomized female (ovariectomized) and male (castrated) mice (n = 6 per group). Samples were compared using two-tailed Student's t test and data points are presented as individual mice with the mean ± SEM (*, $p < 0.05$; **, $p < 0.01$; ***, $p < 0.001$).

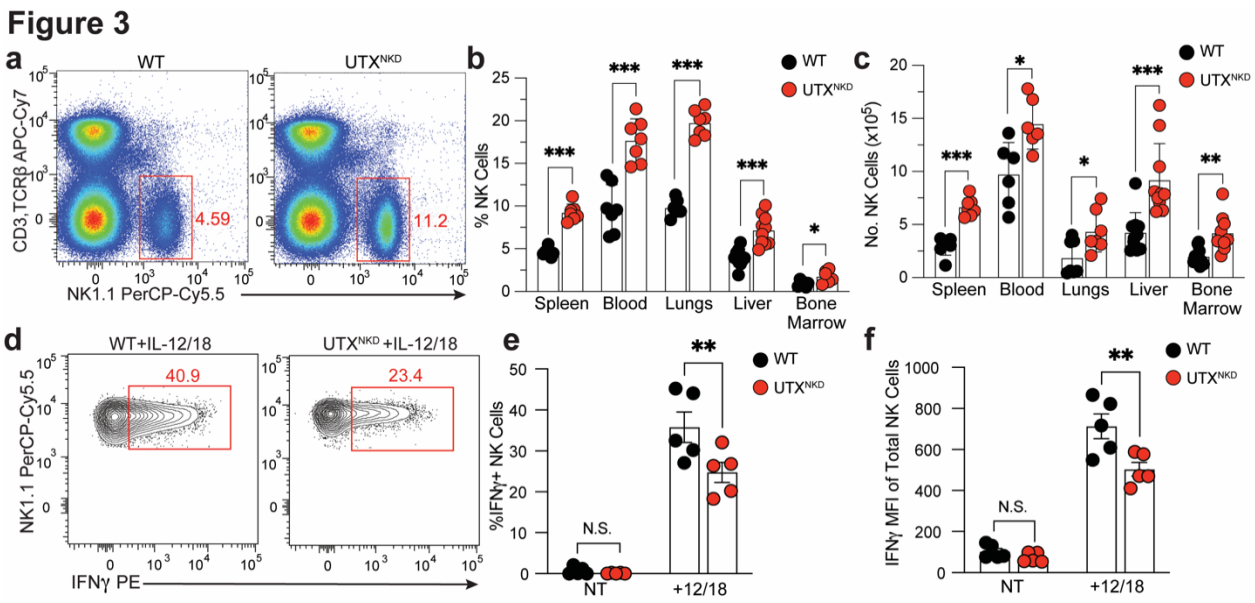

Figure 3: UTX regulates NK cell numbers and IFN-γ expression in NK cells. a) Representative flow cytometry dot plots of splenocytes from WT and UTX^{NKD} mice, gated on NK cells (CD3^{-},TCRβ^{-}NK1.1^{+}). **b)** Percentage and **c)** absolute numbers of NK cells isolated from the spleen, blood, lungs, liver, and bone marrow of WT and UTX^{NKD} mice (n = 6-10 per group). Numbers represent (spleen, lungs and liver – entire organ), (blood - per 1 ml of blood), and (Bone Marrow - 2 femurs per mouse). **d)** Representative contour plots, **e)** frequency, and **f)** MFI of IFN-γ of total NK cells in response to IL-12 (20 ng/ml) and IL-18 (10 ng/ml) stimulation of splenic NK cells from WT and UTX^{NKD} mice for 5 hours *ex vivo* (n = 5 per group). Data are representative of 2-4 independent experiments. Samples were compared using two-tailed Student's t test and data points are presented as individual mice with the mean ± SEM (N.S., Not Significant; *, p <0.05; **, p <0.01; ***, p<0.001).

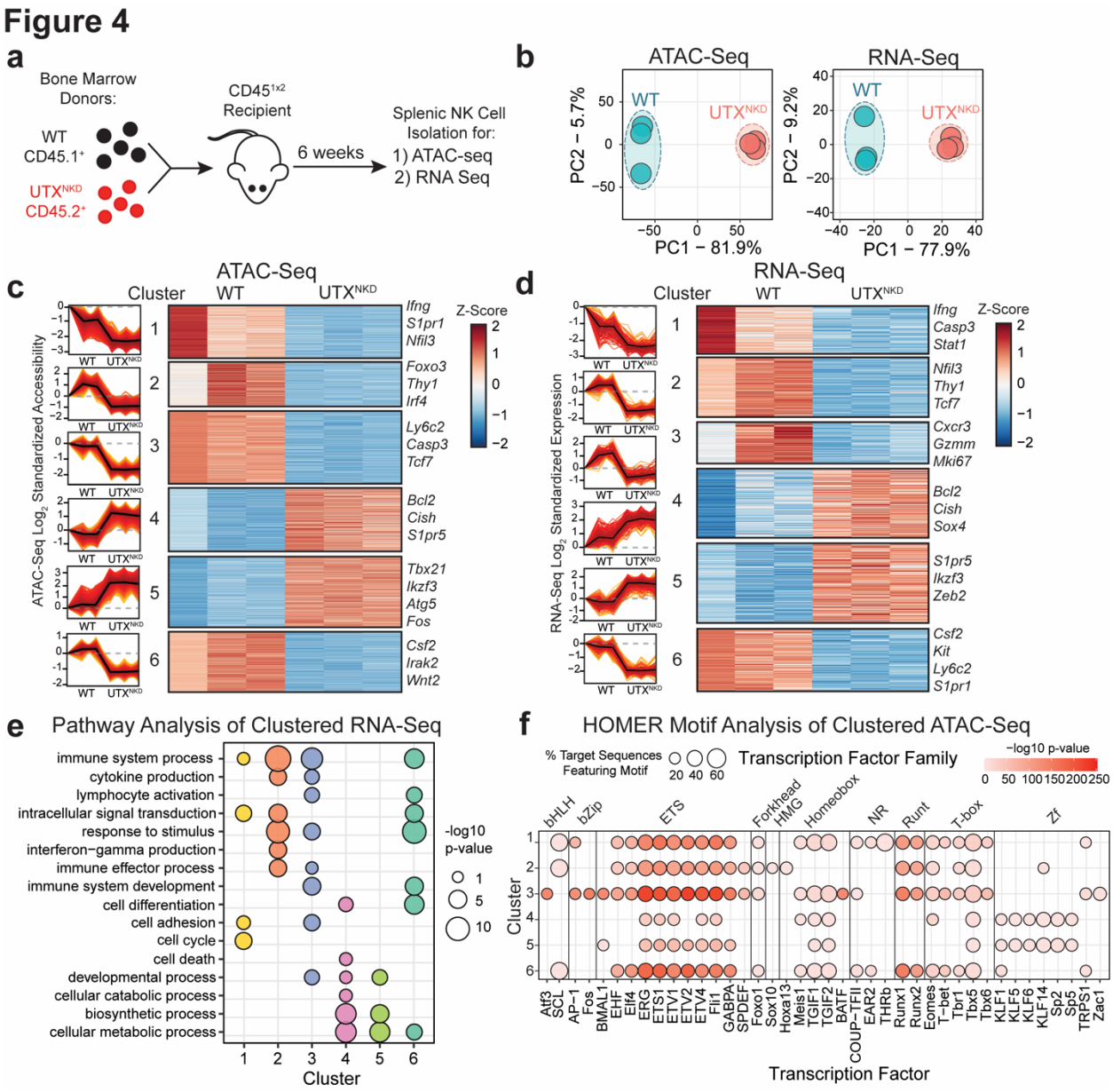

Figure 4: Global changes in NK cell chromatin accessibility and transcription mediated by UTX. a) Schematic of mixed bone marrow chimeras (mBMCs) produced by transferring cells from WT (CD45.1^{+}) and UTX^{NKD} (CD45.2^{+}) bone marrow donors into a lymphodepleted host (CD45^{1x2}) and allowed to reconstitute for 6 weeks. Then NK cells were sorted from spleens of mBMCs for ATAC-seq and RNA-seq library preparation. **b)** Principal component analysis (PCA) of chromatin accessibility (ATAC-seq) and transcriptional (RNA-seq) changes in WT and UTX^{NKD} NK cells at steady state. **c,d)** Line graphs (left) and heatmap (right) of fuzzy c-means

clustered differentially **c)** accessible peaks identified by ATAC-seq and **d)** expressed genes identified by RNA-seq of splenic NK cells from WT:UTX^{NKD} mBMCs (adjusted p-value < 0.05 and membership score > 0.5)**.** Line graphs show mean (black line) and standard deviation (red ribbon) of mean-centered normalized log2 values of significant (FDR and adjusted p-value < 0.05) **c)** peaks of accessibility by ATAC-seq and **d)** gene expression by RNA-seq. **e)** Pathway analysis of significant fuzzy c-means clustered RNA-seq genes using g:Profiler with point size indicating -log10(p-value). **f)** HOMER motif analysis of significant fuzzy c-means clustered ATAC-seq peaks grouped by transcription factor family (top) and transcription factor (bottom). Point size indicates percentage of target sequences featuring motif and red gradient indicates -log10(p-value) of enrichment. All genes displayed in heatmaps met the following threshold of significance: FDR < 0.05, p < 0.05, and Log2FC > 0.5.

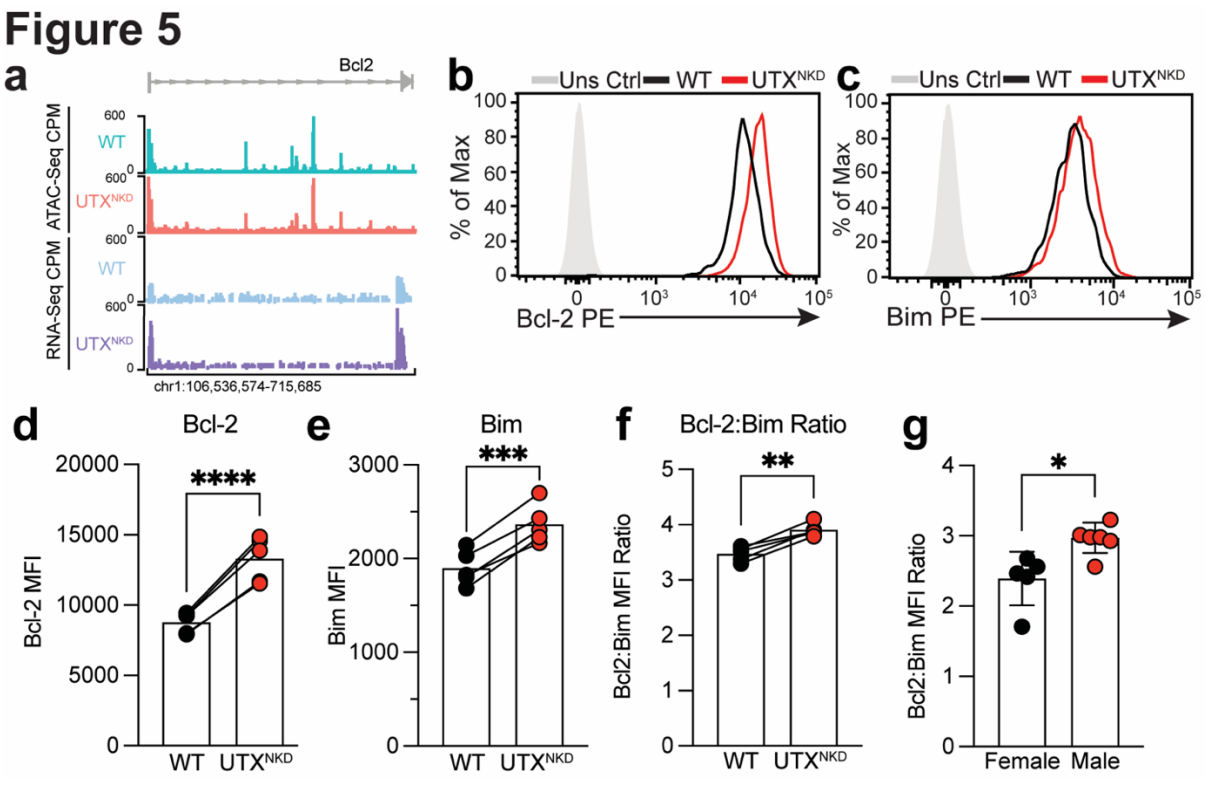

Figure 5: UTX regulates genes involved in apoptosis in NK cells through chromatin remodeling. a) Representative tracks of ATAC-seq signal (WT: green and UTX^{NKD}: red) and RNA-seq transcript signal (WT: blue and UTX^{NKD}: purple) of *Bcl2* in NK cells isolated at rest from WT:UTX^{NKD} mBMCs. Representative histogram of **b)** Bcl-2 and **c)** Bim protein expression, MFI of **d)** Bcl-2, **e)** Bim, and **f)** Bcl-2:Bim ratio from flow cytometric analysis of total peripheral blood NK cells (CD3$^-$TCRβ$^-$NK1.1$^+$) from WT:UTX^{NKD} mBMCs (n = 4). **g)** Bcl-2:Bim MFI ratio of total splenic NK cells (CD3$^-$TCRβ$^-$NK1.1$^+$) from gonadectomized female and male mice (n = 6 per group). Data represent 2-3 independent experiments. Samples were compared using two-tailed Student's t test and data points are presented as individual mice with the mean ± SEM (*, $p < 0.05$; **, $p < 0.01$; ***, $p < 0.001$; ****, $p < 0.0001$).

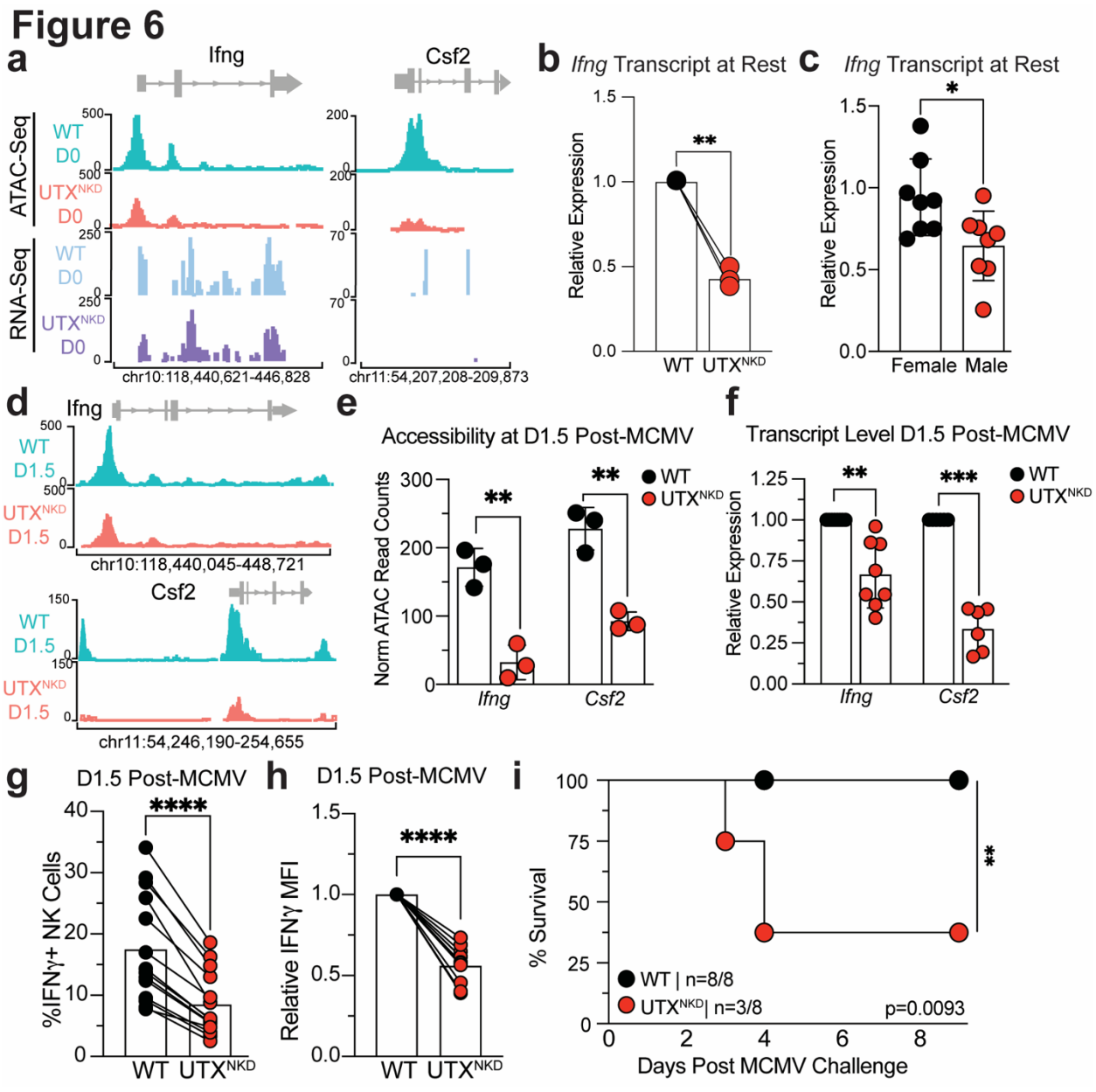

Figure 6: UTX controls the expression of effector genes critical for NK cell-mediated anti-viral immunity. a) Representative tracks of ATAC-seq signal (WT: green and UTX^{NKD}: red) and RNA-seq transcript signal (WT: blue and UTX^{NKD}: purple) of genes involved in NK effector function (*Ifng* and *Csf2)* in NK cells isolated at rest (D0) from WT:UTX^{NKD} mBMCs. **b)** Relative expression of *Ifng* by RT-qPCR of isolated splenic NK cells normalized to WT from WT:UTX^{NKD} mBMCs (n = 3). **c)** Relative expression of *Ifng* transcripts by RT-qPCR in NK cells from female vs. male mice normalized to female mice (C57BL/6; 8 week old, n = 8 per group). **d)**

475 Representative tracks of ATAC-seq signal (WT: green and UTX^{NKD}: red) of genes involved in NK
476 effector function (*Ifng* and *Csf2)* in NK cells isolated at from WT:UTX^{NKD} mBMCs at D1.5 post-
477 MCMV infection. **e)** Normalized read counts of accessibility at a representative peak located in
478 the *Ifng* and *Csf2* loci at D1.5 post-MCMV infection of WT:UTX^{NKD} mBMCs (n = 3). **f)** Expression
479 by RT-qPCR of *Ifng* and *Csf2* transcript levels at D1.5 post-MCMV infection of WT:UTX^{NKD}
480 mBMCs relative to WT (n = 6-8). Flow cytometric analysis of **g)** percent IFN-γ^+ and **h)**
481 normalized IFN-γ MFI relative to WT in splenic NK cells at D1.5 Post MCMV infection of
482 WT:UTX^{NKD} mBMCs (n = 14).**i)** Kaplan-Meier survival curves of WT and UTX^{NKD} mice infected
483 with MCMV (n = 8 per genotype). Mantel-Cox test (**, p=0.0093). Data are representative of 2-3
484 independent experiments. Two-tailed paired Student's t-test was performed, and data points
485 depict individual mice with the mean ± SEM (*, p <0.05; **, p <0.01; ***, p<0.001; ****,
486 p<0.0001).

487

488

489

490

491

492

493

494

495

496

497

498

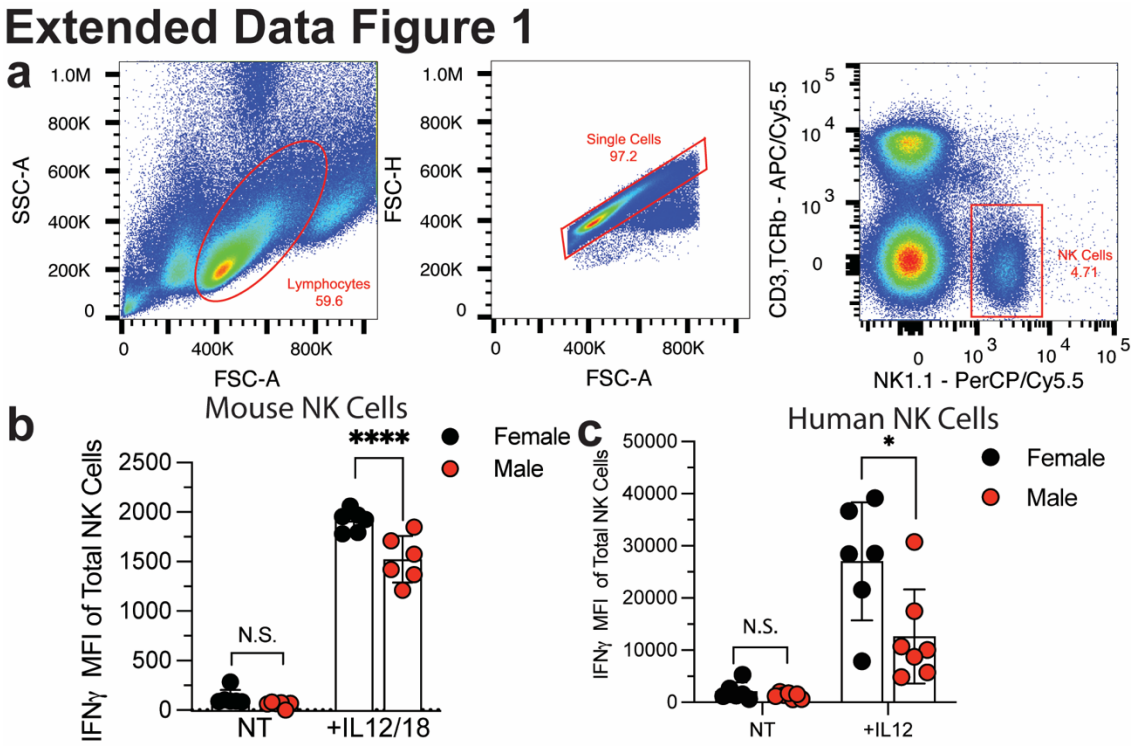

Extended Data Figure 1: Male NK cells from mice and humans produce less IFN-γ than females in response to proinflammatory cytokines. a) Gating strategy for identification of NK cells ($CD3^-$,TCR-β^- $NK1.1^+$) in spleen of C57BL/6 mice. MFI of IFN-γ of NK cells from **b)** mouse stimulated with no treatment (NT) or IL-12 (20 ng/ml) and IL-18 (10 ng/ml) and **c)** human NK cells stimulated with no treatment (NT) IL-12 (10ng/ml). Samples were compared using paired two-tailed Student's t test and data points are presented as individual samples with the mean ± SEM (N.S., Not Significant; *, $p<0.05$; ****, $p<0.0001$).

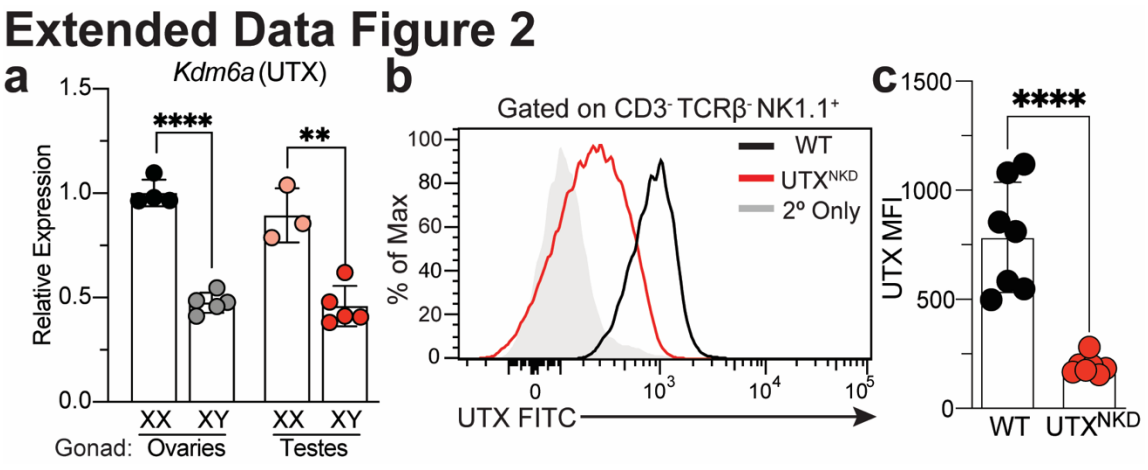

509

510 **Extended Data Figure 2: UTX expression in FCG and UTX^{NKD} mice. a)** Relative expression

511 of *Kdm6a* (UTX) by RT-qPCR from NK cell isolated from spleens of Four Core Genotype (FCG)

512 mice (gonadal female XX n = 5, gonadal female XY n = 5, gonadal male XX n = 3, and gonadal

513 male XY n = 5). **b)** Representative histogram plot and **c)** MFI of UTX protein expression in

514 splenic NK cells (CD3$^-$ TCRβ$^-$ NK1.1$^+$) in WT (*Kdm6a*$^{fl/fl}$ x *Ncr1*$^{cre-}$) and UTX^{NKD} (*Kdm6a*$^{fl/fl}$ x

515 *Ncr1*$^{cre+}$) mice at steady state (n = 7). Samples were compared using paired two-tailed

516 Student's t test and data points are presented as individual mice with the mean ± SEM

517 (**,p<0.01; ****, p<0.0001).

518

519

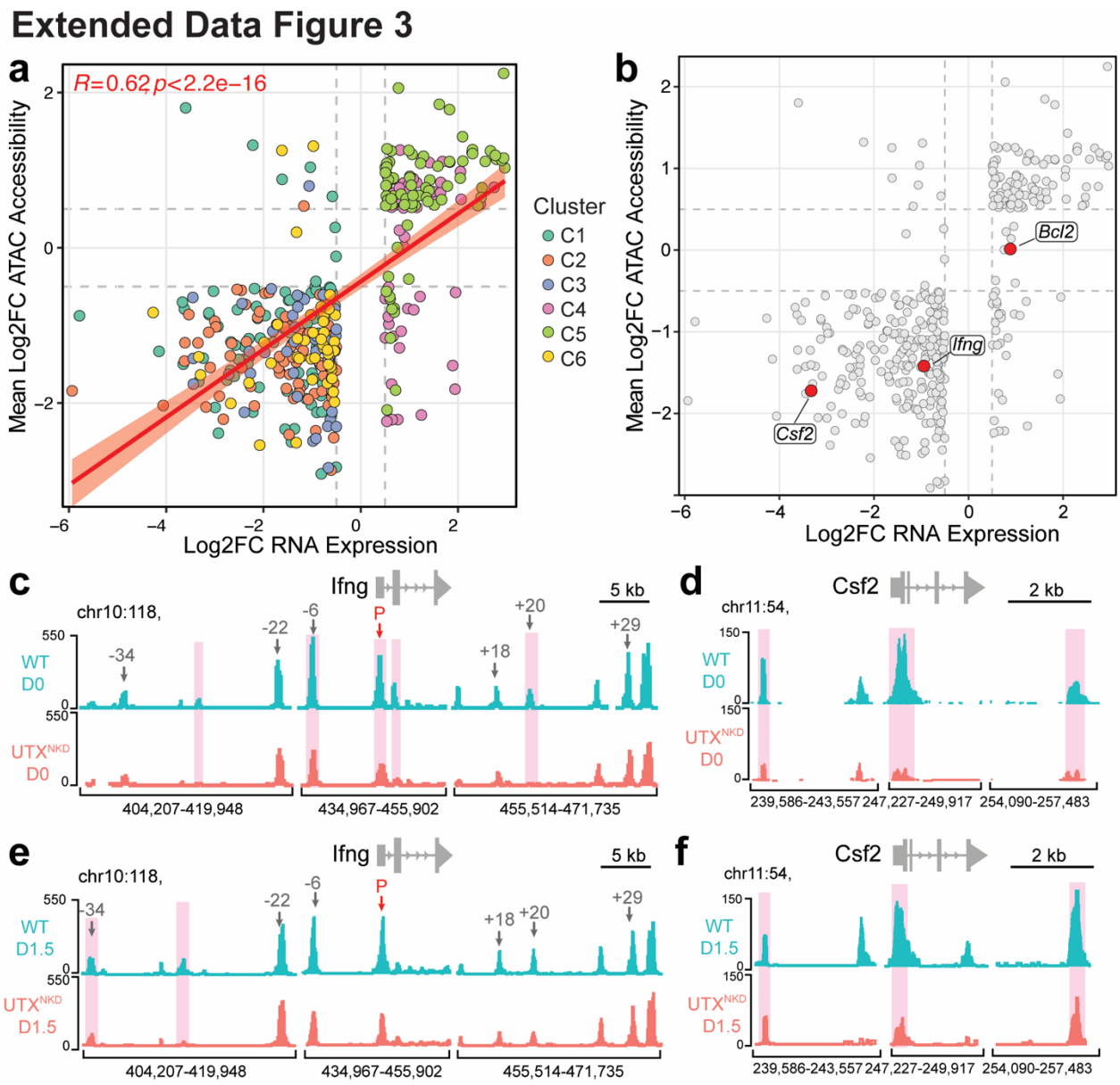

Extended Data Figure 3: Integrative ATAC and RNA seq analysis reveal concomitant changes in chromatin accessibility and transcription mediated by UTX. a) Scatter plot highlighting genes that were differentially accessible and expressed (FDR and adjusted p-value < 0.05) colored by fuzzy c-means cluster (see **Figure 4**). Y-axis depicts mean $\log_2$ fold change of ATAC accessibility peaks and x-axis depicts $\log_2$ fold change of RNA-seq transcript levels. Best fit regression line (red) with standard error (light red ribbon). Positive correlation calculated by Spearman correlation of dataset (R=0.62, $p<2.2\times10^{-16}$). **b)** Specific genes of interest

528 highlighted in red (*Ifng, Csf2, Casp3, Bcl2*) with known roles in NK cell gene programs. **c-f)**
529 Representative tracks of ATAC-seq signal of genes involved in NK effector function **c)** *Ifng* and
530 **d)** *Csf2* in NK cells isolated at rest (D0) and **e)** *Ifng* and **f)** *Csf2* 1.5 days post MCMV infection
531 from WT:UTX^{NKD} mBMCs. Red highlighted areas represent significant differentially accessible
532 regions (FDR and p-value < 0.05).

533

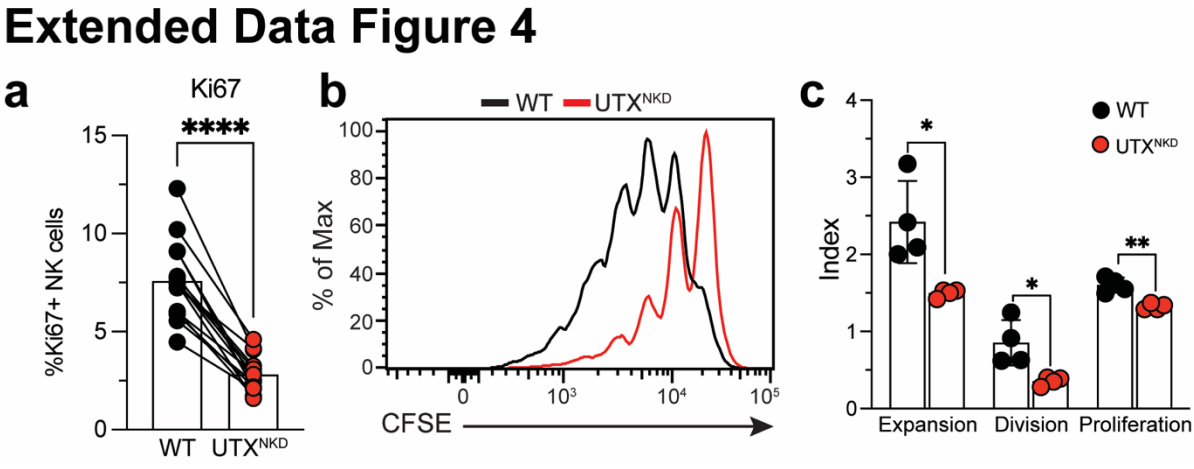

Extended Data Figure 4: UTX deficient NK cells are less proliferative than WT. a) Percentage of Ki67^{+} total NK cells in blood of WT:UTX^{NKD} mBMCs (n=28). **b)** Representative flow cytometry plot and **c)** quantification of CFSE expansion, division and proliferation indexes of CFSE-labeled splenic NK cells from WT:UTX^{NKD} mBMCs stimulated *ex vivo* with IL-15 (50 ng/mL) for 4 days. Data represent 2-3 independent experiments. **a)** Samples were compared using paired and **b-c)** unpaired two-tailed Student's t test and data points are presented as individual mice with the mean ± SEM (*, $p < 0.05$; **, $p < 0.01$).

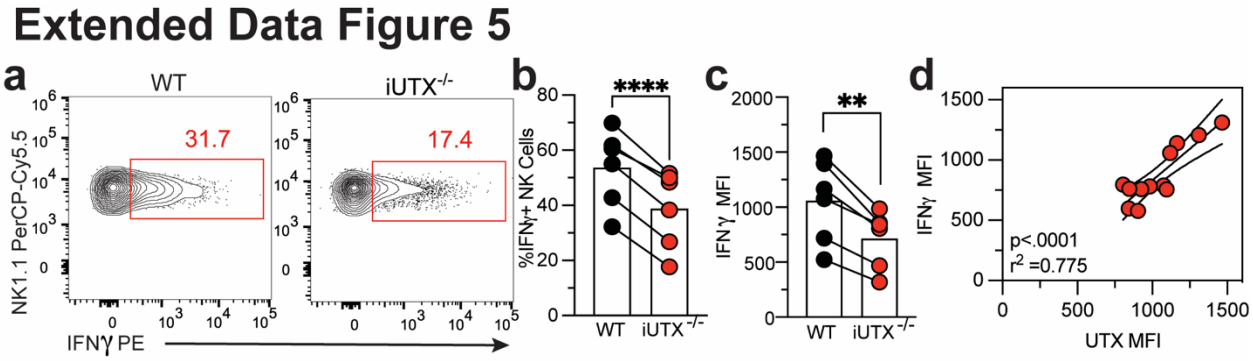

Extended Data Figure 5: UTX regulates IFN-γ production in a dose-dependent manner. WT:UTX$^{-/-}$ mBMCs were produced from WT (CD45.1^{+}) and iUTX$^{-/-}$ (CD45.2^{+}) and treated with tamoxifen for 3 days (1mg/day) prior to MCMV infection. **g)** Representative flow cytometry plot and **h)** %IFN-γ^{+} and **i)** IFN-γ MFI of splenic NK cells at D1.5 post-MCMV infection of WT:iUTX$^{-/-}$ mBMCs (n = 6). **j)** Correlation of IFN-γ vs. UTX MFI of total splenic NK cells (n = 12). Two-tailed correlation of XY data performed. Pearson's r^2 =0.775, and p <0.0001. Data are representative of 2-3 independent experiments. Samples were compared using paired two-tailed Student's t test and data points are presented as individual mice with the mean ± SEM (**, p<0.01; ****, p<0.0001).

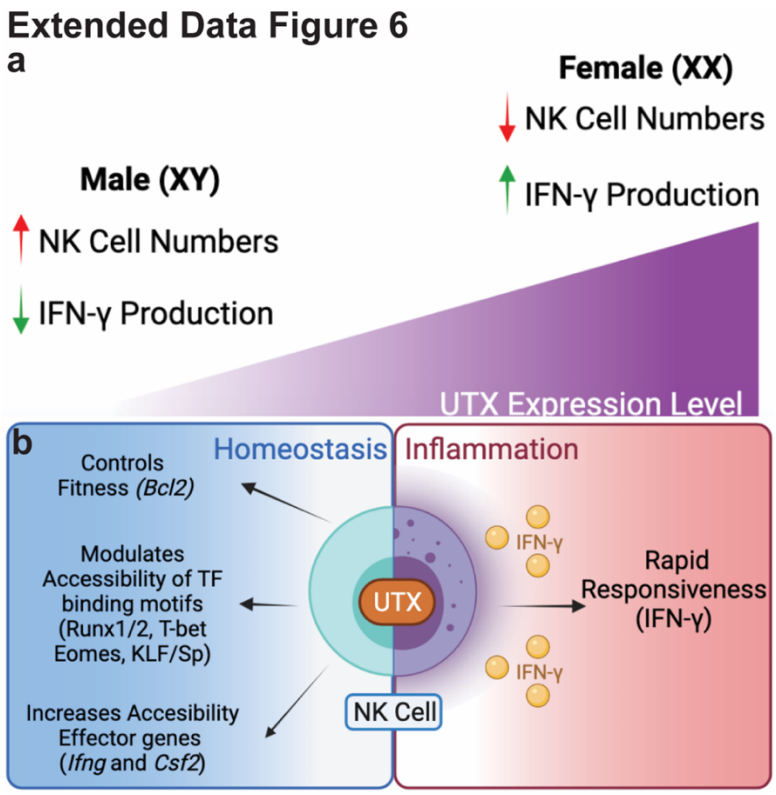

Extended Data Figure 6: Schematic of UTX-mediated sex differences in regulation of NK cell homeostasis and effector function. a) Schematic of how differential UTX expression levels may underlie sexual dimorphism in NK cell composition and function. In male mice, lower UTX levels is associated with expansion of NK cell numbers and decreased NK cell IFN-γ production. **b)** Model in which UTX plays a role to control NK cell fitness and effector function. UTX controls 1) NK cell fitness through restricting Bcl-2 expression, 2) accessibility of TF binding motifs (Runx1/2, T-bet, Eomes, KLF/Sp), and 3) direct changes in chromatin accessibility of effector loci (*Ifng, Csf2*). Ultimately, UTX poises NK cells in an optimal epigenetic state to rapidly respond to viral infection by robust effector molecule production (IFN-γ) resulting in protection against viral infection.

567 **Contact for Reagent and Resource Sharing**

568 Further information and requests for resources and reagents should be directed and will be
569 fulfilled by the Corresponding Authors, Timothy O'Sullivan (tosullivan@mednet.ucla.edu) and
570 Maureen Su (masu@mednet.ucla.edu)

571

572 **Method Details**

573 **Mice**

574 Mice were bred at UCLA in accordance with the guidelines of the institutional Animal Care and
575 Use Committee (IACUC). The following mouse strains were used in this study: C57BL/6
576 (CD45.2) (Jackson Labs, #000664), B6.SJL (CD45.1) (Jackson Labs, #002114), *Rosa26*^{ERT2Cre},
577 *Ncr1*^{Cre}, *Kdm6a*$^{fl/fl}$ and FCG mice. For experiments with gonadectomy, procedure was performed
578 by Jackson Laboratories Surgical Services. For experiments in UTX^{NKD} mice, only female mice
579 were used to control for Y chromosome and sex hormone independent effects. Thus,
580 experiments were conducted using 6-8 week old age-matched females in accordance with
581 approved institutional protocols. For comparisons between male and female WT, we used 6-8
582 weeks age-matched littermates. Mixed bone marrow chimeras (mBMCs) were generated by
583 depleting host CD45.1 x CD45.2 mice by intraperitoneal (i.p.) injection of busulfan (1mg/mL) at
584 20mg/kg for 3 consecutive days, which were then reconstituted 24 hours later with various
585 mixtures of bone marrow cells from WT (CD45.1) and knockout (CD45.2) donor mice in the
586 presence of an anti-NK1.1 antibody (at 1 mg/ml; clone: PK136) to deplete any remaining mature
587 NK cells.

588

589 *MCMV infection*

590 MCMV (Smith) was serially passaged through BALB/c hosts three times, and then salivary
591 gland viral stocks were prepared with a dounce homogenizer for dissociating the salivary glands
592 of infected mice 3 weeks after infection. Experimental mice in studies were infected with MCMV

593 by i.p. injection of 7.5 x 10^3 plaque-forming units (PFU) in 0.5 mL of PBS. Mice were monitored
594 and weighed daily and sacrificed when body weight dropped over 20% from initial weight.
595
596 *Isolation and enrichment of mouse NK cells*
597 Mouse spleens, livers, lungs, and blood were harvested and prepared into single cell
598 suspensions as described previously[57]. Splenic single cell suspensions were lysed in red blood
599 cell lysis buffer and resuspended in EasySep™ buffer (Stemcell). To avoid depleting Ly6C$^+$ NK
600 cells we developed a custom antibody cocktail as follows: splenocytes were labeled with 10 µg
601 per spleen of biotin conjugated antibodies against CD3 (17A2), CD19 (6D5), CD8 (53-6.7),
602 CD88 (20/70), Ly6G (1A8), SiglecF (S17007L), TCRβ (H57-597), CD20 (SA275A11), CD172a
603 (P84) and magnetically depleted from total splenocyte suspensions with the use of anti-biotin
604 coupled magnetic beads (Biolegend)[58].
605
606 *Ex vivo stimulation of lymphocytes*
607 ~5 x 10^5 NK cells were stimulated for 5 hours in complete RPMI media (RPMI 1640 + 25 mM
608 HEPES + 10% FBS, 1% L-glutamine, 1% 200 mM sodium pyruvate, 1% MEM-NEAA, 1%
609 penicillin-streptomycin, 0.5% sodium bicarbonate, 0.01% 55 mM 2-mercaptoethanol) , Brefeldin
610 A (1:1000; BioLegend) and Monensin (2uM; BioLegend) with or without recombinant mouse IL-
611 12 (20 ng/ml; Peprotech) and recombinant mouse IL-18 (10ng/ml; Peprotech). Cells were
612 cultured in complete RPMI media alone as a negative control (No Treatment or NT).
613
614 *Human NK cell culture and Stimulation*
615 Human peripheral blood mononuclear cells (PBMCs) from anonymous healthy donors were
616 obtained from leukoreduction filters after platelet apheresis from the UCLA Virology Core. NK
617 cells were isolated using the EasySep Human NK Cell Isolation Kit (Stem Cell Technologies)
618 following manufacturer instructions. Following isolation, cells were maintained in 24-well G-Rex

619 plates (Wilson Wolf) in NK MACS media (Miltenyi Biotech) supplemented with human IL-2 (100
620 IU/mL, Peprotech) and human IL-15 (20 ng/mL, Peprotech) at a plating density of $5x10^6$ cells
621 per well. For cytokine stimulation, 14 d IL-2/IL-15 activated human NK cells were plated with
622 K562 leukemia cells at an effector:target (E:T) ratio of 2.5:1 in addition to human IL-2 (100
623 IU/mL, Peprotech), human IL-15 (20 ng/mL, Peprotech), human IL-12 (10 ng/mL, Peprotech),
624 and/or human IL-18 (100 ng/mL, Peprotech) in complete RPMI media (Thermo Fisher). NK cells
625 were stimulated with cytokines for 16 h before analysis by flow cytometry.
626
627 *Proliferation assays*
628 CellTrace™ CFSE (Thermo) stock solution was prepared per the manufacturers' instructions
629 and diluted at 1:10,000 in 37C PBS. Isolated NK cells were incubated in 0.5mL of diluted CFSE
630 solution for 5 minutes at 37C. The solution was quenched with 10X the volume of complete
631 RPMI media. Cells were then washed and plated with 50 ng/ml of recombinant mouse IL-15
632 (Peprotech) and cultured for 4 days to assess proliferation. Flow cytometry was used to quantify
633 CFSE dilution 4 days post-stimulation. Samples were compared to levels of CFSE labeled on
634 Day 0. FlowJo's proliferation tool was used to model and measure number of divisions in
635 addition to expansion, division, and proliferation indices.
636
637 *Flow Cytometry and Cell Sorting*
638 Cells were analyzed for cell-surface markers using fluorophore-conjugated antibodies
639 (BioLegend, eBioscience). Cell surface staining was performed in FACS Buffer (2% FBS and 2
640 mM EDTA in PBS) and intracellular staining was performed by fixing and permeabilizing using
641 the eBioscience Foxp3/Transcription Factor kit for intranuclear proteins or BD Cytofix/Cytoperm
642 kits for cytokines. Flow cytometry was performed using the Attune NxT Acoustic Focusing
643 cytometer and data were analyzed with FlowJo software (TreeStar). NK cells were identified as
644 $CD3^-$ $TCR\beta^-$ $NK1.1^+$ cells: see gating strategy in Extended Data Fig. 1. Cell surface and

645 intracellular staining was performed using the following fluorophore-conjugated antibodies:
646 CD45.1 (A20), CD45.2 (104), NK1.1 (PK136), TCRβ (H57-597), CD3 (17A2), IFN-γ (XMG1.2),
647 Ly6C (HK1.4), BCL2 (BCL/10C4), UTX (N2C1 - GeneTex), Goat anti-rabbit H&L (Abcam -
648 ab6717), BIM (c34c5), CD90 (30-H12), Ki-67 (16A8). Isolated splenic NK cells were sorted
649 using Aria-H Cytometer to > 95% purity.
650
651 *RNA-seq and ATAC-seq library construction and analysis*
652 RNA was isolated from the cells using RNeasy Mini kit (Qiagen) and used to generate RNA-seq
653 libraries followed by sequencing using Illumina HighSeq 4000 platform (single end, 50bp). The
654 reads were mapped with HISAT2 (version 2.2.1) to the mouse genome (mm10). The counts for
655 each gene were obtained by HtSeq[59], in print, online at doi:10.1093/bioinformatics/btu638).
656 Differential expression analyses were carried out using DESeq2[60] (version 1.24.0) with default
657 parameters. Genes with adjusted p value <0.05 were considered significantly differentially
658 expressed. Sequencing depth normalized counts were used to plot the expression values for
659 individual genes.
660 ATAC-seq libraries were produced by the Applied Genomics, Computation, and
661 Translational Core Facility at Cedars Sinai in the following manner: 50,000 cells per sample
662 were lysed to collect nuclei and treated with Tn5 transposase (Illumina) for 30 minutes at 37°C
663 with gentle agitation. The DNA was isolated with DNA Clean & Concentrator Kit (Zymo) and
664 PCR amplified and barcoded with NEBNext High-Fidelity PCR Mix (New England Biolabs) and
665 unique dual indexes (Illumina). The ATAC-Seq library amplification was confirmed by real-time
666 PCR, and additional barcoding PCR cycles were added as necessary while avoiding
667 overamplification. Amplified ATAC-Seq libraries were purified with DNA Clean & Concentrator
668 Kit (Zymo). The purified libraries were quantified with Kapa Library Quant Kit (KAPA
669 Biosystems) and quality assessed on 4200 TapeStation System (Agilent). The libraries were

670 pooled based on molar concentrations and sequenced on an Illumina HighSeq 4000 platform
671 (paired end, 100bp).
672 ATAC-seq fastq files were trimmed to remove low-quality reads and adapters using
673 Cutadapt[61] (version 2.3). The reads were aligned to the reference mouse genome (mm10) with
674 bowtie2[62] (version 2.2.9). Peak calling was performed with MACS2[63] (version 2.1.1). The peaks
675 from all samples were merged into a single bed file, peaks from different samples that were
676 closer than 10bp were merged into a single peak. HTseq[59] (version 0.9.1) was used to count the
677 number of reads that overlap each peak per sample. The peak counts were analyzed with
678 DESeq2[60] (version 1.24.0) to identify differentially accessible genomic regions. Peaks with
679 adjusted p-value < 0.05 were considered significantly differentially accessible. The peak counts
680 were visualized with Integrated Genome Browser, (version 9.1.8).
681 Fuzzy c-means clustering was used for both ATAC-seq and RNA-seq using significant
682 (p-value and FDR <0.05, Log_2FC +/- 0.5) normalized counts generated from DESeq2. MFuzz
683 package (version 3.14) within R was used to perform this analysis into 6 clusters with a
684 membership score of >0.5. The differentially accessible ATAC peaks were analyzed using the
685 findMotifsGenome.pl function from HOMER[37] (version 4.9.1) of each cluster to identify enriched
686 cis-regulatory motifs of transcription factors. Pathway analysis of clustered RNA-seq data was
687 performed using g:Profiler using the g:GOSt function. Top relevant pathways were selected
688 from KEGG Biological Pathways and Gene Ontology Pathways (Biological Processes and
689 Molecular Function).
690
691 *Statistical Analyses*
692 For graphs, data are shown as mean ± SEM, and unless otherwise indicated, statistical
693 differences were evaluated using a Student's t-test. For Kaplan-Meir survival curve, samples
694 were compared using the Log-rank (Mantel-Cox) test with correction for testing multiple
695 hypotheses. A p-value < 0.05 was considered significant. Graphs were produced and statistical

696 analyses were performed using GraphPad Prism and ggplot2 library in R. Spearman Correlation
697 on best fit regression line was performed using ggpubr library in R.
698
699 *Data Availability*
700 Sequencing datasets are accessible from GEO with accession number GSE185065. Data can
701 be accessed by reviewers using the access token ilqlqswavvqhtir.
702

References

1 Wilkinson, N. M., Chen, H. C., Lechner, M. G. & Su, M. A. Sex Differences in Immunity. *Annu Rev Immunol*, doi:10.1146/annurev-immunol-101320-125133 (2022).

2 Klein, S. L. & Flanagan, K. L. Sex differences in immune responses. *Nat Rev Immunol* **16**, 626-638, doi:10.1038/nri.2016.90 (2016).

3 Pardue, M.-L. & Wizemann, T. M. Exploring the biological contributions to human health: does sex matter? (2001).

4 Gianella, S., Tran, S. M., Morris, S., Vargas, M., Porrachia, M., Oliveira, M. F., Lada, S., Zhao, M., Ellsworth, G. B., Mathad, J. S. & Wilkin, T. Sex Differences in CMV Replication and HIV Persistence During Suppressive ART. *Open Forum Infect Dis* **7**, ofaa289, doi:10.1093/ofid/ofaa289 (2020).

5 Takahashi, T. & Iwasaki, A. Sex differences in immune responses. *Science* **371**, 347-348, doi:10.1126/science.abe7199 (2021).

6 Abdullah, M., Chai, P. S., Chong, M. Y., Tohit, E. R., Ramasamy, R., Pei, C. P. & Vidyadaran, S. Gender effect on in vitro lymphocyte subset levels of healthy individuals. *Cell Immunol* **272**, 214-219, doi:10.1016/j.cellimm.2011.10.009 (2012).

7 Lee, B. W., Yap, H. K., Chew, F. T., Quah, T. C., Prabhakaran, K., Chan, G. S., Wong, S. C. & Seah, C. C. Age- and sex-related changes in lymphocyte subpopulations of healthy Asian subjects: from birth to adulthood. *Cytometry* **26**, 8-15, doi:10.1002/(sici)1097-0320(19960315)26:1<8::aid-cyto2>3.0.co;2-e (1996).

8 Melzer, S., Zachariae, S., Bocsi, J., Engel, C., Loffler, M. & Tarnok, A. Reference intervals for leukocyte subsets in adults: Results from a population-based study using 10-color flow cytometry. *Cytometry B Clin Cytom* **88**, 270-281, doi:10.1002/cyto.b.21234 (2015).

9 Patin, E., Hasan, M., Bergstedt, J., Rouilly, V., Libri, V., Urrutia, A., Alanio, C., Scepanovic, P., Hammer, C., Jonsson, F., Beitz, B., Quach, H., Lim, Y. W., Hunkapiller, J., Zepeda, M., Green, C., Piasecka, B., Leloup, C., Rogge, L., Huetz, F., Peguillet, I., Lantz, O., Fontes, M., Di Santo, J. P., Thomas, S., Fellay, J., Duffy, D., Quintana-Murci, L., Albert, M. L. & Milieu Interieur, C. Natural variation in the parameters of innate immune cells is preferentially driven by genetic factors. *Nat Immunol* **19**, 302-314, doi:10.1038/s41590-018-0049-7 (2018).

10 Huang, Z., Chen, B., Liu, X., Li, H., Xie, L., Gao, Y., Duan, R., Li, Z., Zhang, J., Zheng, Y. & Su, W. Effects of sex and aging on the immune cell landscape as assessed by single-cell transcriptomic analysis. *Proc Natl Acad Sci U S A* **118**, doi:10.1073/pnas.2023216118 (2021).

11 Fang, H., Disteche, C. M. & Berletch, J. B. X Inactivation and Escape: Epigenetic and Structural Features. *Front Cell Dev Biol* **7**, 219, doi:10.3389/fcell.2019.00219 (2019).

12 Chen, X., Watkins, R., Delot, E., Reliene, R., Schiestl, R. H., Burgoyne, P. S. & Arnold, A. P. Sex difference in neural tube defects in p53-null mice is caused by differences in the complement of X not Y genes. *Dev Neurobiol* **68**, 265-273, doi:10.1002/dneu.20581 (2008).

13 Smith-Bouvier, D. L., Divekar, A. A., Sasidhar, M., Du, S., Tiwari-Woodruff, S. K., King, J. K., Arnold, A. P., Singh, R. R. & Voskuhl, R. R. A role for sex chromosome complement in the female bias in autoimmune disease. *J Exp Med* **205**, 1099-1108, doi:10.1084/jem.20070850 (2008).

14 Hammer, Q., Ruckert, T. & Romagnani, C. Natural killer cell specificity for viral infections. *Nat Immunol* **19**, 800-808, doi:10.1038/s41590-018-0163-6 (2018).

15 Orange, J. S. Natural killer cell deficiency. *J Allergy Clin Immunol* **132**, 515-525, doi:10.1016/j.jaci.2013.07.020 (2013).

752 16 Biron, C. A., Byron, K. S. & Sullivan, J. L. Severe herpesvirus infections in an adolescent
753 without natural killer cells. *N Engl J Med* **320**, 1731-1735,
754 doi:10.1056/NEJM198906293202605 (1989).
755 17 Scalzo, A. A., Fitzgerald, N. A., Simmons, A., La Vista, A. B. & Shellam, G. R. Cmv-1, a
756 genetic locus that controls murine cytomegalovirus replication in the spleen. *J Exp Med*
757 **171**, 1469-1483 (1990).
758 18 Bukowski, J. F., Warner, J. F., Dennert, G. & Welsh, R. M. Adoptive transfer studies
759 demonstrating the antiviral effect of natural killer cells in vivo. *J Exp Med* **161**, 40-52
760 (1985).
761 19 Welsh, R. M., Brubaker, J. O., Vargas-Cortes, M. & O'Donnell, C. L. Natural killer (NK)
762 cell response to virus infections in mice with severe combined immunodeficiency. The
763 stimulation of NK cells and the NK cell-dependent control of virus infections occur
764 independently of T and B cell function. *J Exp Med* **173**, 1053-1063 (1991).
765 20 Brown, M. G., Dokun, A. O., Heusel, J. W., Smith, H. R., Beckman, D. L., Blattenberger,
766 E. A., Dubbelde, C. E., Stone, L. R., Scalzo, A. A. & Yokoyama, W. M. Vital involvement
767 of a natural killer cell activation receptor in resistance to viral infection. *Science* **292**,
768 934-937, doi:10.1126/science.1060042 (2001).
769 21 Daniels, K. A., Devora, G., Lai, W. C., O'Donnell, C. L., Bennett, M. & Welsh, R. M.
770 Murine cytomegalovirus is regulated by a discrete subset of natural killer cells reactive
771 with monoclonal antibody to Ly49H. *J Exp Med* **194**, 29-44 (2001).
772 22 Bukowski, J. F., Woda, B. A., Habu, S., Okumura, K. & Welsh, R. M. Natural killer cell
773 depletion enhances virus synthesis and virus-induced hepatitis in vivo. *J Immunol* **131**,
774 1531-1538 (1983).
775 23 Bancroft, G. J., Shellam, G. R. & Chalmer, J. E. Genetic influences on the augmentation
776 of natural killer (NK) cells during murine cytomegalovirus infection: correlation with
777 patterns of resistance. *J Immunol* **126**, 988-994 (1981).
778 24 Welsh, R. M., Dundon, P. L., Eynon, E. E., Brubaker, J. O., Koo, G. C. & O'Donnell, C. L.
779 Demonstration of the antiviral role of natural killer cells in vivo with a natural killer cell-
780 specific monoclonal antibody (NK 1.1). *Nat Immun Cell Growth Regul* **9**, 112-120 (1990).
781 25 Shellam, G. R., Allan, J. E., Papadimitriou, J. M. & Bancroft, G. J. Increased
782 susceptibility to cytomegalovirus infection in beige mutant mice. *Proc Natl Acad Sci U S*
783 *A* **78**, 5104-5108 (1981).
784 26 Menees, K. B., Earls, R. H., Chung, J., Jernigan, J., Filipov, N. M., Carpenter, J. M. &
785 Lee, J. K. Sex- and age-dependent alterations of splenic immune cell profile and NK cell
786 phenotypes and function in C57BL/6J mice. *Immun Ageing* **18**, 3, doi:10.1186/s12979-
787 021-00214-3 (2021).
788 27 Mujal, A. M., Delconte, R. B. & Sun, J. C. Natural Killer Cells: From Innate to Adaptive
789 Features. *Annu Rev Immunol* **39**, 417-447, doi:10.1146/annurev-immunol-101819-
790 074948 (2021).
791 28 Lauwerys, B. R., Renauld, J. C. & Houssiau, F. A. Synergistic proliferation and activation
792 of natural killer cells by interleukin 12 and interleukin 18. *Cytokine* **11**, 822-830,
793 doi:10.1006/cyto.1999.0501 (1999).
794 29 Nakaya, M., Tachibana, H. & Yamada, K. Effect of estrogens on the interferon-gamma
795 producing cell population of mouse splenocytes. *Biosci Biotechnol Biochem* **70**, 47-53,
796 doi:10.1271/bbb.70.47 (2006).
797 30 Berletch, J. B., Ma, W., Yang, F., Shendure, J., Noble, W. S., Disteche, C. M. & Deng, X.
798 Escape from X inactivation varies in mouse tissues. *PLoS Genet* **11**, e1005079,
799 doi:10.1371/journal.pgen.1005079 (2015).
800 31 Arnold, A. P. Four Core Genotypes and XY* mouse models: Update on impact on SABV
801 research. *Neurosci Biobehav Rev* **119**, 1-8, doi:10.1016/j.neubiorev.2020.09.021 (2020).

32 Sciume, G., Mikami, Y., Jankovic, D., Nagashima, H., Villarino, A. V., Morrison, T., Yao, C., Signorella, S., Sun, H. W., Brooks, S. R., Fang, D., Sartorelli, V., Nakayamada, S., Hirahara, K., Zitti, B., Davis, F. P., Kanno, Y., O'Shea, J. J. & Shih, H. Y. Rapid Enhancer Remodeling and Transcription Factor Repurposing Enable High Magnitude Gene Induction upon Acute Activation of NK Cells. *Immunity* **53**, 745-758 e744, doi:10.1016/j.immuni.2020.09.008 (2020).

33 Shih, H. Y., Sciume, G., Mikami, Y., Guo, L., Sun, H. W., Brooks, S. R., Urban, J. F., Jr., Davis, F. P., Kanno, Y. & O'Shea, J. J. Developmental Acquisition of Regulomes Underlies Innate Lymphoid Cell Functionality. *Cell* **165**, 1120-1133, doi:10.1016/j.cell.2016.04.029 (2016).

34 Miller, S. A., Mohn, S. E. & Weinmann, A. S. Jmjd3 and UTX play a demethylase-independent role in chromatin remodeling to regulate T-box family member-dependent gene expression. *Mol Cell* **40**, 594-605, doi:10.1016/j.molcel.2010.10.028 (2010).

35 Dembele, D. & Kastner, P. Fuzzy C-means method for clustering microarray data. *Bioinformatics* **19**, 973-980, doi:10.1093/bioinformatics/btg119 (2003).

36 Raudvere, U., Kolberg, L., Kuzmin, I., Arak, T., Adler, P., Peterson, H. & Vilo, J. g:Profiler: a web server for functional enrichment analysis and conversions of gene lists (2019 update). *Nucleic Acids Res* **47**, W191-W198, doi:10.1093/nar/gkz369 (2019).

37 Heinz, S., Benner, C., Spann, N., Bertolino, E., Lin, Y. C., Laslo, P., Cheng, J. X., Murre, C., Singh, H. & Glass, C. K. Simple combinations of lineage-determining transcription factors prime cis-regulatory elements required for macrophage and B cell identities. *Mol Cell* **38**, 576-589, doi:10.1016/j.molcel.2010.05.004 (2010).

38 Rapp, M., Lau, C. M., Adams, N. M., Weizman, O. E., O'Sullivan, T. E., Geary, C. D. & Sun, J. C. Core-binding factor beta and Runx transcription factors promote adaptive natural killer cell responses. *Sci Immunol* **2**, doi:10.1126/sciimmunol.aan3796 (2017).

39 Simonetta, F., Pradier, A. & Roosnek, E. T-bet and Eomesodermin in NK Cell Development, Maturation, and Function. *Front Immunol* **7**, 241, doi:10.3389/fimmu.2016.00241 (2016).

40 Presnell, J. S., Schnitzler, C. E. & Browne, W. E. KLF/SP Transcription Factor Family Evolution: Expansion, Diversification, and Innovation in Eukaryotes. *Genome Biol Evol* **7**, 2289-2309, doi:10.1093/gbe/evv141 (2015).

41 Viant, C., Guia, S., Hennessy, R. J., Rautela, J., Pham, K., Bernat, C., Goh, W., Jiao, Y., Delconte, R., Roger, M., Simon, V., Souza-Fonseca-Guimaraes, F., Grabow, S., Belz, G. T., Kile, B. T., Strasser, A., Gray, D., Hodgkin, P. D., Beutler, B., Vivier, E., Ugolini, S. & Huntington, N. D. Cell cycle progression dictates the requirement for BCL2 in natural killer cell survival. *J Exp Med* **214**, 491-510, doi:10.1084/jem.20160869 (2017).

42 Louis, C., Souza-Fonseca-Guimaraes, F., Yang, Y., D'Silva, D., Kratina, T., Dagley, L., Hediyeh-Zadeh, S., Rautela, J., Masters, S. L., Davis, M. J., Babon, J. J., Ciric, B., Vivier, E., Alexander, W. S., Huntington, N. D. & Wicks, I. P. NK cell-derived GM-CSF potentiates inflammatory arthritis and is negatively regulated by CIS. *J Exp Med* **217**, doi:10.1084/jem.20191421 (2020).

43 Kramer, B., Knoll, R., Bonaguro, L., ToVinh, M., Raabe, J., Astaburuaga-Garcia, R., Schulte-Schrepping, J., Kaiser, K. M., Rieke, G. J., Bischoff, J., Monin, M. B., Hoffmeister, C., Schlabe, S., De Domenico, E., Reusch, N., Handler, K., Reynolds, G., Bluthgen, N., Hack, G., Finnemann, C., Nischalke, H. D., Strassburg, C. P., Stephenson, E., Su, Y., Gardner, L., Yuan, D., Chen, D., Goldman, J., Rosenstiel, P., Schmidt, S. V., Latz, E., Hrusovsky, K., Ball, A. J., Johnson, J. M., Koenig, P. A., Schmidt, F. I., Haniffa, M., Heath, J. R., Kummerer, B. M., Keitel, V., Jensen, B., Stubbemann, P., Kurth, F., Sander, L. E., Sawitzki, B., Deutsche, C.-O. I., Aschenbrenner, A. C., Schultze, J. L. & Nattermann, J. Early IFN-alpha signatures and persistent dysfunction are distinguishing

852 features of NK cells in severe COVID-19. *Immunity* **54**, 2650-2669 e2614,
853 doi:10.1016/j.immuni.2021.09.002 (2021).
854 44 Cook, K. D., Shpargel, K. B., Starmer, J., Whitfield-Larry, F., Conley, B., Allard, D. E.,
855 Rager, J. E., Fry, R. C., Davenport, M. L., Magnuson, T., Whitmire, J. K. & Su, M. A. T
856 Follicular Helper Cell-Dependent Clearance of a Persistent Virus Infection Requires T
857 Cell Expression of the Histone Demethylase UTX. *Immunity* **43**, 703-714,
858 doi:10.1016/j.immuni.2015.09.002 (2015).
859 45 Beyaz, S., Kim, J. H., Pinello, L., Xifaras, M. E., Hu, Y., Huang, J., Kerenyi, M. A., Das,
860 P. P., Barnitz, R. A., Herault, A., Dogum, R., Haining, W. N., Yilmaz, O. H., Passegue,
861 E., Yuan, G. C., Orkin, S. H. & Winau, F. The histone demethylase UTX regulates the
862 lineage-specific epigenetic program of invariant natural killer T cells. *Nat Immunol* **18**,
863 184-195, doi:10.1038/ni.3644 (2017).
864 46 Mitchell, J. E., Lund, M. M., Starmer, J., Ge, K., Magnuson, T., Shpargel, K. B. &
865 Whitmire, J. K. UTX promotes CD8(+) T cell-mediated antiviral defenses but reduces T
866 cell durability. *Cell Rep* **35**, 108966, doi:10.1016/j.celrep.2021.108966 (2021).
867 47 Pomeroy, C., Delong, D., Clabots, C., Riciputi, P. & Filice, G. A. Role of interferon-
868 gamma in murine cytomegalovirus infection. *J Lab Clin Med* **132**, 124-133,
869 doi:10.1016/s0022-2143(98)90007-5 (1998).
870 48 Bosselut, R. Pleiotropic Functions of H3K27Me3 Demethylases in Immune Cell
871 Differentiation. *Trends Immunol* **37**, 102-113, doi:10.1016/j.it.2015.12.004 (2016).
872 49 Wang, S. P., Tang, Z., Chen, C. W., Shimada, M., Koche, R. P., Wang, L. H., Nakadai,
873 T., Chramiec, A., Krivtsov, A. V., Armstrong, S. A. & Roeder, R. G. A UTX-MLL4-p300
874 Transcriptional Regulatory Network Coordinately Shapes Active Enhancer Landscapes
875 for Eliciting Transcription. *Mol Cell* **67**, 308-321 e306, doi:10.1016/j.molcel.2017.06.028
876 (2017).
877 50 Maj, T., Wang, W., Crespo, J., Zhang, H., Wang, W., Wei, S., Zhao, L., Vatan, L., Shao,
878 I., Szeliga, W., Lyssiotis, C., Liu, J. R., Kryczek, I. & Zou, W. Oxidative stress controls
879 regulatory T cell apoptosis and suppressor activity and PD-L1-blockade resistance in
880 tumor. *Nat Immunol* **18**, 1332-1341, doi:10.1038/ni.3868 (2017).
881 51 Cribbs, A., Hookway, E. S., Wells, G., Lindow, M., Obad, S., Oerum, H., Prinjha, R. K.,
882 Athanasou, N., Sowman, A., Philpott, M., Penn, H., Soderstrom, K., Feldmann, M. &
883 Oppermann, U. Inhibition of histone H3K27 demethylases selectively modulates
884 inflammatory phenotypes of natural killer cells. *J Biol Chem* **293**, 2422-2437,
885 doi:10.1074/jbc.RA117.000698 (2018).
886 52 Kruidenier, L., Chung, C. W., Cheng, Z., Liddle, J., Che, K., Joberty, G., Bantscheff, M.,
887 Bountra, C., Bridges, A., Diallo, H., Eberhard, D., Hutchinson, S., Jones, E., Katso, R.,
888 Leveridge, M., Mander, P. K., Mosley, J., Ramirez-Molina, C., Rowland, P., Schofield, C.
889 J., Sheppard, R. J., Smith, J. E., Swales, C., Tanner, R., Thomas, P., Tumber, A.,
890 Drewes, G., Oppermann, U., Patel, D. J., Lee, K. & Wilson, D. M. A selective jumonji
891 H3K27 demethylase inhibitor modulates the proinflammatory macrophage response.
892 *Nature* **488**, 404-408, doi:10.1038/nature11262 (2012).
893 53 van der Heiden, M., van Zelm, M. C., Bartol, S. J. W., de Rond, L. G. H., Berbers, G. A.
894 M., Boots, A. M. H. & Buisman, A. M. Differential effects of Cytomegalovirus carriage on
895 the immune phenotype of middle-aged males and females. *Sci Rep* **6**, 26892,
896 doi:10.1038/srep26892 (2016).
897 54 Van Laarhoven, P. M., Neitzel, L. R., Quintana, A. M., Geiger, E. A., Zackai, E. H.,
898 Clouthier, D. E., Artinger, K. B., Ming, J. E. & Shaikh, T. H. Kabuki syndrome genes
899 KMT2D and KDM6A: functional analyses demonstrate critical roles in craniofacial, heart
900 and brain development. *Hum Mol Genet* **24**, 4443-4453, doi:10.1093/hmg/ddv180
901 (2015).

55 Rezvani, K. Adoptive cell therapy using engineered natural killer cells. *Bone Marrow Transplant* **54**, 785-788, doi:10.1038/s41409-019-0601-6 (2019).

56 Angelo, L. S., Hogg, G. D., Abeynaike, S., Bimler, L., Vargas-Hernandez, A. & Paust, S. Phenotypic and Functional Plasticity of CXCR6(+) Peripheral Blood NK Cells. *Front Immunol* **12**, 810080, doi:10.3389/fimmu.2021.810080 (2021).

57 Weizman, O. E., Adams, N. M., Schuster, I. S., Krishna, C., Pritykin, Y., Lau, C., Degli-Esposti, M. A., Leslie, C. S., Sun, J. C. & O'Sullivan, T. E. ILC1 Confer Early Host Protection at Initial Sites of Viral Infection. *Cell* **171**, 795-808 e712, doi:10.1016/j.cell.2017.09.052 (2017).

58 Riggan, L., Ma, F., Li, J. H., Fernandez, E., Nathanson, D. A., Pellegrini, M. & O'Sullivan, T. E. The transcription factor Fli1 restricts the formation of memory precursor NK cells during viral infection. *Nat Immunol*, doi:10.1038/s41590-022-01150-0 (2022).

59 Anders, S., Pyl, P. T. & Huber, W. HTSeq--a Python framework to work with high-throughput sequencing data. *Bioinformatics* **31**, 166-169, doi:10.1093/bioinformatics/btu638 (2015).

60 Love, M. I., Huber, W. & Anders, S. Moderated estimation of fold change and dispersion for RNA-seq data with DESeq2. *Genome Biol* **15**, 550, doi:10.1186/s13059-014-0550-8 (2014).

61 Kechin, A., Boyarskikh, U., Kel, A. & Filipenko, M. cutPrimers: A New Tool for Accurate Cutting of Primers from Reads of Targeted Next Generation Sequencing. *J Comput Biol* **24**, 1138-1143, doi:10.1089/cmb.2017.0096 (2017).

62 Langmead, B. & Salzberg, S. L. Fast gapped-read alignment with Bowtie 2. *Nat Methods* **9**, 357-359, doi:10.1038/nmeth.1923 (2012).

63 Zhang, Y., Liu, T., Meyer, C. A., Eeckhoute, J., Johnson, D. S., Bernstein, B. E., Nusbaum, C., Myers, R. M., Brown, M., Li, W. & Liu, X. S. Model-based analysis of ChIP-Seq (MACS). *Genome Biol* **9**, R137, doi:10.1186/gb-2008-9-9-r137 (2008).